POLITECNICO DI TORINO
Master's Degree in Biomedical Engineering
Bionanotechnologies

Master' s Degree Thesis

PRODUCTION OF MULTIRESPONSIVE THIN FILMS CONTAINING CARBON DOTS

Supervisors:
Prof. Alberto Tagliaferro
Dr. Francesca Frascella
Dr. Mattia Bartoli

Candidate:
Claudia Suriano

Academic year 2023/2024

Contents

Abstract

Carbon dots (CDs) are an emerging carbon nanosized species with high photoluminescence quantum yields. CDs were accidentally discovered in 2004 during the isolation and purification of single-walled carbon nanotubes synthesized by arc-discharge methods. Since their discovery, various synthesis methods employing various precursors have been developed, that fall into two broad classes: top-down and bottom-up approaches. Also, CDs based composite materials have been studied widely for applications in many fields.

CDs are typically quasi-spherical nanoparticles with an amorphous to nanocrystalline structure, containing sp2/sp3 carbon, oxygen/nitrogen-based groups, and superficial chemical groups.

Carbon dots have attracted a broad interest in several fields due to their unique combination of optical properties, exceptional biocompatibility, minimal toxicity, great aqueous solubility, cost-effectiveness, simple synthesis, easy functionalization. These characteristics have spread their use from bioimaging, biosensing, chemical sensing to nanomedicine, antibacterial therapy, and optoelectronic devices.

This thesis work is focused on exploited high-fluorescence CDs as a component of a composite material to create multifunctional films. CDs were synthetized by ultrasonic-assisted method using Citric Acid (CA) and p-Phenylendiamine (p-DPA) as precursors. Different molar ratios of the precursors were used to find the right compromise between high photoluminescence and scalability. The film is obtained from pre-functionalised CDs, a photopolymerizable resin and a photoinitiator under UV light exposure. Both CDs and multifunctional films have been characterised with spectroscopic techniques, AFM, TGA, FTIR and swelling test.

The films obtained could be used either to monitor interfaces for biomedical applications or to release active substances/CDs or a combination of the previous ones. In each case the main source of information is the variation of photoluminescence (PL) intensity throughout the film life cycle.

1 Introduction

1.1 Carbon dots

CDs are an emerging subclass of carbon nanoparticles. PL stands out as one of the most captivating properties of CDs.

CDs were discovered in 2004 during the isolation and purification of single-walled carbon nanotubes synthesised through arc-discharge methods [1]. In 2006, the first attempt was made to functionalise CDs[2]. In 2008, another significant breakthrough was made with the synthesis of CDs by thermal decomposition of organic precursors such as citrate salts [3]. In 2010, the production of highly crystalline CDs demonstrated for the first time the PL size dependence in these materials [4]. These key developments in the evolution of CDs have been pivotal milestones for subsequent research efforts.

Due to the wide variety of structures and PL mechanisms associated with CDs, CDs nomenclature represent a relevant issue. CDs may be referred to also as carbon quantum dots, carbon nanodots or carbon nanoparticles. Generally, it is used the term CDs to describe all quasi-spherical carbon nanomaterials < 10 nm [5].

1.1.1 Classification

The classification can be based either on the characteristic structural elements or on the production methods or on the PL mechanisms. The structure of CDs generally consists of a core (layers of graphene), a less crystalline shell and exposed functionalities (responsible for interactions) [6] as shown in Figure 1 .

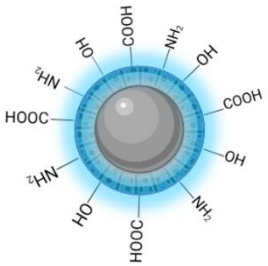

Figure 1 - Core-shell structure of CDs.

According to the chemical structure of core and shell regions, CDs can be classified in Graphene Quantum Dots (GQDs), hetero atom-doped Graphene Quantum Dots (xGQDs), Carbon Quantum Dots (CQDs), Carbon Nanodots (CNDs), and Carbon Polymer Dots (CPDs). It is useful to introduce the carbon nitride quantum dots

(CNQDs) which are like GQDs, with nitrogen-doped graphene units instead of oxygen-based ones [7].

The synthetic routes for preparing CDs are principally divided into top–down and bottom–up procedures. The top–down approach transforms the massive carbon precursors into a mixture of particles comprising CDs. In the bottom–up approach small organic molecules are combined to form CDs.

Considering the main mechanisms of PL, which will be discussed upon in the following sections, it is possible to group in categories CDs that exhibit similar mechanisms [8].

- Quantum Confinement Effects (QCEs), or conjugated π-domains are shared by GQDs and CQDs.
- Surface states is typical of CNDs.
- Crosslink-Enhanced Emission (CEE) effect is typical of CPDs.

The PL classification is closely related to structural features and synthesis methods. Therefore, the most appropriate approach to the identification of a CD type is to perform chemical, structural and PL analysis simultaneously.

1.1.2 Structure

The study of the structure of CDs remains a subject of ongoing research, mainly due to their complexity and variability resulting from the multitude of precursors available for their synthesis. Understanding the structure becomes fundamental, particularly for critical applications. For instance, the approval of CDs for biomedical applications in humans is highly unlikely without a well-defined structure.

CDs are classified in several structural categories which are strictly correlated with the PL features and the synthesis approaches. Figure 2 shows a comprehensive classification.

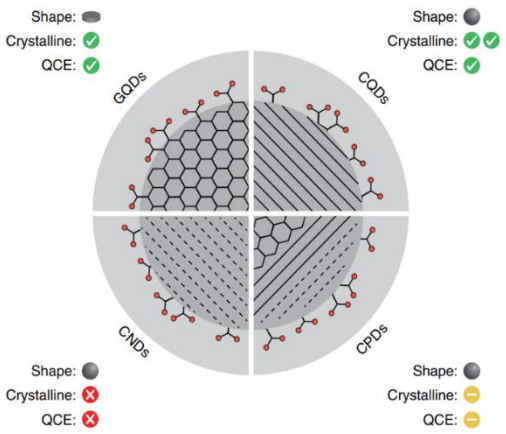

Figure 2 - Schematic illustration of CDs based on the structure, shape, and PL characteristics. (Reproduced with permission, source [11])

The structural interpretation of GQDs in Figure 3 is based on the Lerf-Klinowsky's model of graphite oxide [9]. GQDs are generally discoidal particles, made of graphene layers with highly oxidized functional groups on the edges. They have an average lattice parameter of 0.24 nm [10]. The layers of GQDs can assume various shapes, including triangular, rectangular, hexagonal, and dendrimeric, thereby influencing the optical properties of the particle [7]. Introduction of heteroatoms to GQDs, either during or after synthesis, results in the formation of xGQDs.

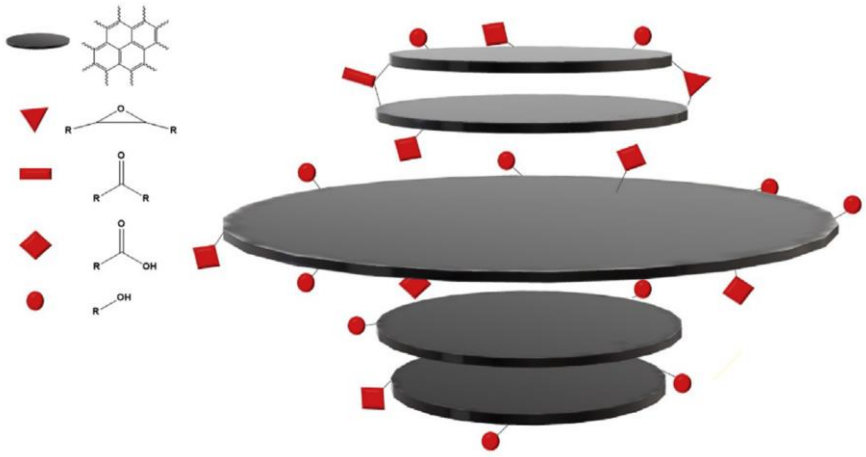

Figure 3 - Schematic structure of GQDs. (Reproduced with permission, source [10])

CQNDs present nitrogen atoms into graphene-like layers. As reported in Figure 4 [10], the core consists of carbon, oxygen, and nitrogen atoms. CQNDs possess various surface groups and their structure possess more order than GQDs.

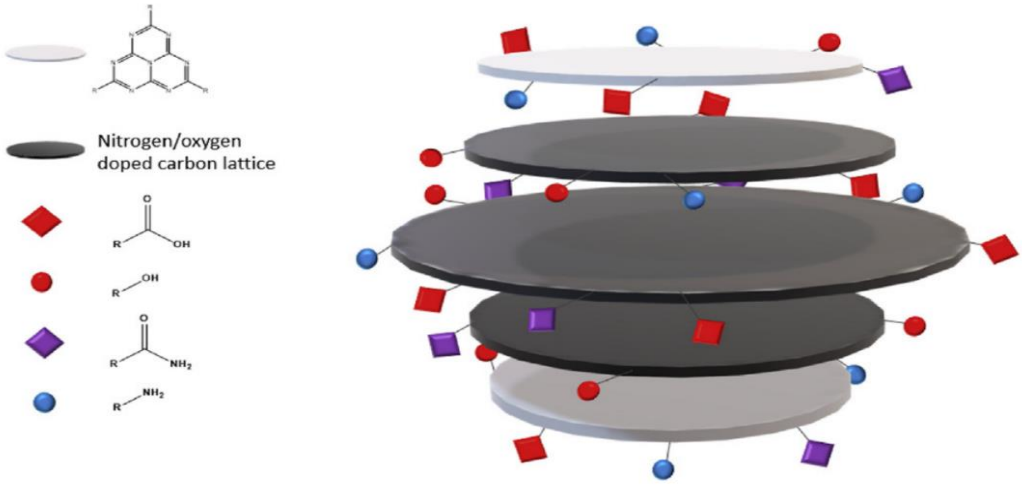

Figure 4 - Schematic structure of CQNDs. (Reproduced with permission, source [10])

CQDs are nearly spherical particles with a crystalline structure resulting from the arrangement and interaction of graphene planes within the material. Functional

groups are also present on the surface of CQDs [11]. The standard spacing between the crystalline planes is approximately 0.34 nm [12].

CNDs are quasi-spherical particles and possess a non-crystalline carbonized structure with surface functional groups [11].

CPDs are quasi-spherical nanoparticles composed of aggregated polymer chains or core-shell structures where the core is carbon-based, while the shell is made up of polymer chains [12]. CPDs can be synthesized through monomers condensation or bulk material degradation. The former method produces CPDs with more well-defined structures and properties. Mintz et al. [10] synthesized and characterized CPDs derived from citric acid (CA) and 1,2-diaminobenzene (DPA). The CPDs exhibit a unique 3D structure due to the presence of single C-N bond between the aromatic units of DPA and the aliphatic units of CA. This allows the polymer chains to rotate and pack into this structure. As a result, the CPDs demonstrate superior particle stability and lower crystallinity compared to GQDs and CQNDs. Figure 5 provides an insight into CPDs structural features.

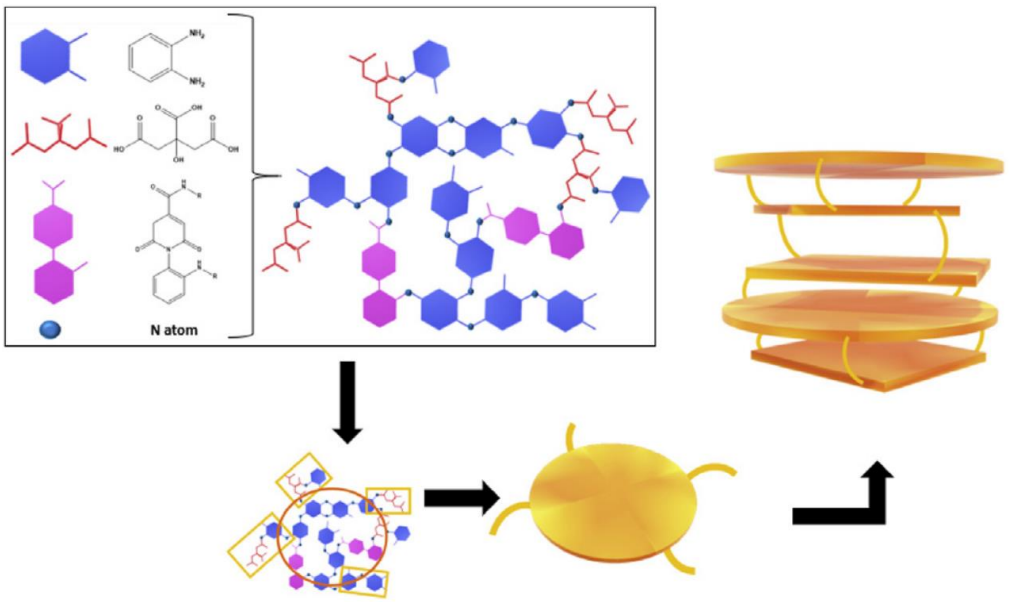

Figure 5 - Schematic structure of PCDs produced using CA and DPA. (Reproduced with permission, source [10])

CPDs synthesized in this thesis work should be like those obtained by Mintz et al. [10], as the same precursors and synthesis method have been used with the exception of the argon gas flux during the sonication.

1.1.3 Synthesis Methods

1.1.3.1 Top-down methods

The first methods used were Top-down. They involve breaking down larger carbon structures such as graphite powder, carbon rods, carbon fibres, carbon nanotubes or carbon black (Figure 6).

The carbon materials have a perfect sp2 carbon structure and do not exhibit fluorescence due to the absence of a band gap. Therefore, their structure and size must be adjusted using top-down approaches [12].

Arc discharge was the very first method used to produce CDs [1]. This method involves the formation of an arc discharge between two graphite electrodes at a specific voltage. The high temperature and high pressure around the arc lead to the vaporisation of the carbon atoms from the electrodes. The resulting carbon atoms then nucleate in the vapour, forming nanoparticles.

The electrochemical process leads to exfoliation of a carbon anode, resulting in the formation of CDs. Oxidation caused by radical species, or the presence of electrolytes induces structural defects that embrittle the material. This leads to the fracture of the carbon anode. A high redox potential between ±1.5 V and ±3 V is essential to oxidise C-C bonds and water molecules and to produce hydroxyl and oxygen radicals that contribute to the exfoliation of the anode [13].

In chemical oxidation, the C-C bonds of high-carbon materials can be broken by using strong oxidants (e.g. sulfuric acid and nitric acid) [14].

Hydrothermal/solvothermal methods use a synthesis solution prepared by dissolving a carbon-containing material in either water or organic solvents, depending on the method used. The resulting solution is then placed in an autoclave, which is crucial for maintaining high pressure. The autoclave is heated at high temperature to induce the thermochemical degradation and rearrangement of the precursors. Varying temperature, solvent and reaction time allows a controlled production of CDs.

The laser ablation method uses a high-energy laser to vaporize carbon atoms from carbon-rich material surface. This process results in the nucleation of carbon atoms, ultimately leading to the formation of CDs [15].

Pyrolysis is a process in which organic material is heated to high temperatures in a vacuum or inert atmosphere. The material is progressively heated, degraded and carbonised until CDs are obtained [16].

While these methodologies can generate substantial quantities of CDs, they typically involve harsh conditions, such as high applied voltage or the use of

chemical oxidants, prolonged synthesis durations, and necessitate post-synthetic procedures for fine-tuning the optoelectronic properties.

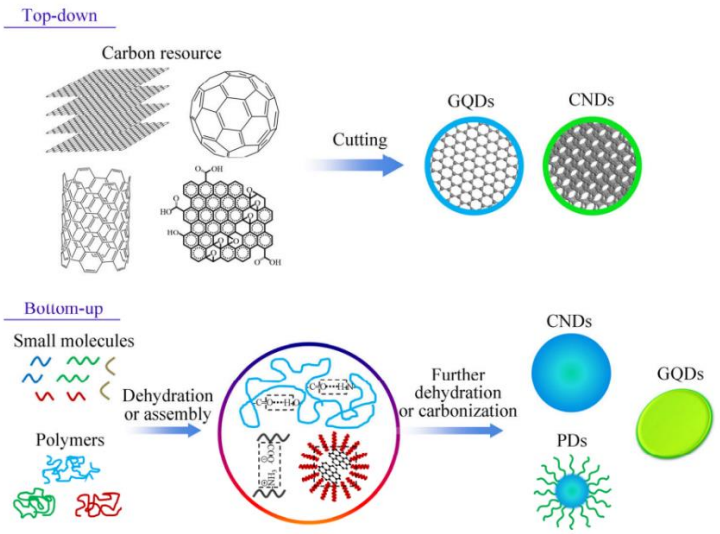

Figure 6 - Schematic representation of CDs synthesis approaches. (Reproduced with permission, source [12])

1.1.3.2 Bottom-up methods

Bottom-up approaches consist of synthetising C-dots starting from molecular precursors like organic monomers and/or polymers (Figure 6).

Bottom-up syntheses are more versatile considering the multitude of molecular precursors available, the multiple choices of thermal treatments, the quicker reaction times, the more uniform properties in the final material and the fluorescence of CDs on a large scale. It is difficult to control these formation processes, resulting in CDs with polydispersity. There are many bottom-up approaches.

In Combustion/Thermal method, carbon dots are synthesized through the combustion or thermal decomposition of carbon-containing precursors.

Microwave-assisted synthesis involves the exposure of precursor materials to microwave irradiation. The method is known for its quick reaction times.

Hydrothermal synthesis involves the reaction of carbon-containing precursors in a high-pressure, high-temperature aqueous environment. This method often results in the formation of carbon dots with well-defined sizes and enhanced properties.

Electrochemical methods apply an electric potential to induce the formation of carbon dots on electrodes or in an electrolyte.

Self-assembly methods rely on the spontaneous organization of precursor molecules into carbon dots without the need for external forces. This method often results in well-structured carbon dots with controlled properties.

Carbonization in a microreactor involves the controlled carbonization of precursor materials within a microscale reactor.

Enhanced Hydrothermal (Microwave-Hydrothermal and Plasma-Hydrothermal) methods combine hydrothermal synthesis with additional energy sources like microwaves or plasma.

Ultrasound Assisted synthesis involves the application of high-frequency ultrasound waves to promote the formation of carbon dots. The cavitation effect induced by ultrasound contributes to the efficient synthesis of carbon dots with unique properties.

1.1.3.3 Surface functionality and passivation

The size, degree of graphitisation, exposed functional groups, doping and degree of carbonisation of CDs can be controlled by selecting appropriate precursors and synthesis conditions. Surface modifications, such as the addition of other active groups or passivation, can be employed with to enhance CDs fluorescence (Figure 7).

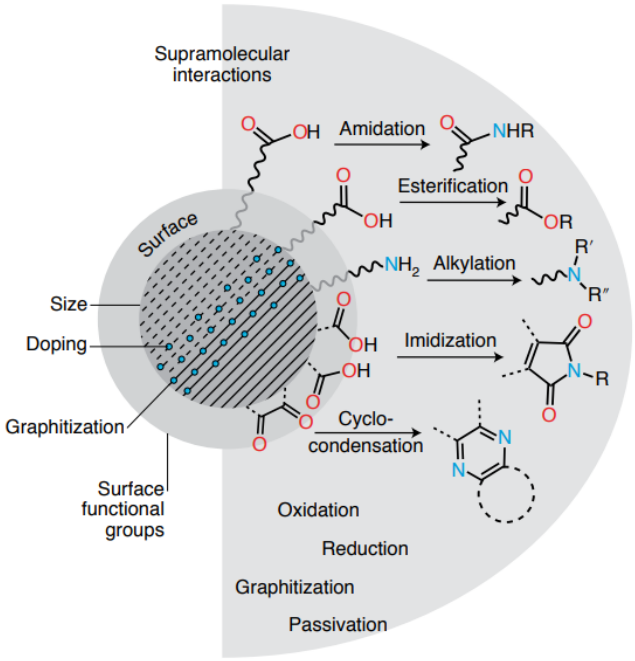

Figure 7 - Schematic illustration of CDs properties control approaches. (Reproduced with permission, source [11])

1.1.4 Properties

1.1.4.1 Optical absorption

CDs reveal strong optical absorption in the UV region with a long tail that extends into the visible range even to the NIR region. The correlation between the absorption spectrum and the electron transition of both the core and functional groups of CDs is illustrated in Figure 8 [17].

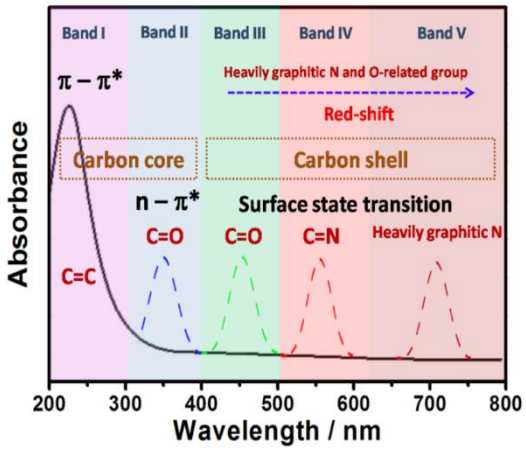

Figure 8 - A schematic illustration of the relationship between the absorption spectrum and electron transition of CDs (Reproduced with permission, source [17]).

Absorbance in the bands below 300 nm is commonly attributed to the $\pi \rightarrow \pi^*$ transition of the C=C bonds in the core and sp2 networks as in graphene. The peaks between 300 and 400 nm are usually assigned to the $n \rightarrow \pi^*$ transition of the C=O or C=N bonds present in the core.

The absorption bands above 400 nm are caused by the surface state transition. The red-shifted UV-vis absorption spectrum from ca. 420 nm to NIR spectral region is attributed to the addition of graphitic nitrogen into the carbon sp2 lattice and O-containing functional group (hydroxyl, carboxyl, and epoxy) on CDs surface.

The emission peak position is always related to the excitation wavelength, which is known as wavelength-dependent behaviour.

1.1.4.2 Fluorescence

Tho origins of the luminescent mechanism of CDs are mainly ascribed to:

1. Quantum confinement/size effect
2. Conjugated structures
3. Surface state
4. Crosslink-enhanced emission (CEE) effect
5. Self-trapped excitons
6. Edge defects
7. Free zigzag sites

8. Multi-emissive centres
9. Synthesis parameters

Quantum confinement is a phenomenon related to the nanometric size of the particle, occurring when the Bohr radius of the exciton is bigger than the particle's average size. The increase of core size leads to an increase in the extent of the π-electron system, which in turn reduces the energy gap between the valence band and conduction band. As the CD size decreases, the HOMO-LUMO energy gap increases, resulting in the emission of photons in the UV region and an improvement in the QY [18].

Conjugated structures exhibit a diffuse electron cloud over a significant portion of their core due to the π-system of sp2 domains, making them highly susceptible to the fluorescence phenomenon. As the extent of the π-electron domain increases, the energy gap of $\pi \rightarrow \pi^*$ transitions decreases. Surface states also contribute to a small energy gap. These observations demonstrate the significant impact of conjugation on the fluorescence properties of molecules. Larger π-domains reduce the HOMO-LUMO gap and cause a red shift in the fluorescence emission peak. [19]

Therefore, the red-shifted emission of CDs is derived from the enlarged π -electron domain or the increase in size of CDs.

The surface state involves the degree of surface oxidation, surface functional groups and chemical composition. [20]

Surface oxidation creates defects that lead to various emission sites on the CDs surface. The greater the number of surface defects there are, the more excitons (i.e. electrons and holes) can be trapped. Consequently, the radiation from the recombination of trapped excitons results in red-shifted emission.

The different CDs emissions (blue, green and red fluorescence) result from the radiative recombination of the excited electrons from the $n \rightarrow \pi^*$ transition of C=O, creating numerous new energy levels between $n \rightarrow \pi^*$ gaps. The band gap decreases with increasing surface oxidation on CDs surface, resulting in a fluorescence redshift.

Surface functional groups such as C=O and C=N groups, also known as the molecular state, can tune the fluorescence of CDs. The O-related groups (C=O) and N-related groups (C=N) can introduce two new energy levels and produce new electron transitions. Consequently, the red-shift emission will occur when the electrons in C=O or C=N groups related defect states return to the HOMO.

Self-trapped excitons occur when a photoexcited exciton induces a distortion or reorientation in the molecular geometry, binding with the exciton to create a polaron. This results in reduced energy and mobility, which in turn reduces the relaxation and degradation process. The emission tends to shift to longer wavelengths and lower energy over time. [21]

Oxygen-related functional groups at the edge of CDs or two overlapped spectral bands with intrinsic and extrinsic states cause special edge defects that can tune the fluorescence of CDs. The size of the defect increases with the oxygen content on the surface, resulting in a more significant red shift of the fluorescence. [22]

The electronic structure of graphene quantum dots (GQDs) is significantly affected by their edge structure. The blue fluorescence of GQDs arises from free zigzag sites that have a carbene-like triplet ground state. The blue emission results from the decay of activated electrons from the lowest unoccupied molecular orbital (LUMO) to the highest occupied molecular orbital (HOMO). [23]

Cutting graphene sheets along different crystallographic directions produces diverse types of edges, including armchair and zigzag edges. The type of edge plays a crucial role in determining the electronic, magnetic, and optical properties of the GQD. A higher fraction of zigzag edges results in a smaller energy gap than those with a predominantly armchair-edge ribbon of similar width.

The fluorescence of CDs is tuneable and arises from multiple small emissive molecules hybridized on the emissive carbon cores. In general, the blue-green emission mainly results from the graphitic core, while the long-wavelength emission is related to different C=O and C=N surface functional groups existing in the molecular residues. Conjugated molecular residues containing N and O act as various emission centres. [24]

The phenomenon of CEE was firstly described by Tao et al. [25]. They compared the fluorescence emission of poly(ethylenimine) with CPDs-derived materials produced by the degradation and crosslinking of the polymer. An increase in fluorescence emission was observed, which was suggested to be due to the formation of a rigid structure that prevented the intramolecular rotations and vibrations promoting the fluorescence emission. Reduced mobility of the covalent bond caused by steric hindrance or supramolecular interactions can decrease the nonradiative relaxation and enhance the fluorescence of CPDs. [25]

The fluorescent intensity of CDs increases with increasing temperature that influences the kinetic of the nucleation and growth of CDs and the formation of the shell. At higher concentrations of CDs, the interparticle distance decreases leading to increased interaction and resulting in the red-shift and decrease in fluorescent intensity due to the self-absorption. The surface functional groups of CDs have a close relationship with the behaviour of pH through protonation/deprotonation. Deprotonation induces electrostatic doping/charging of CDs and shifts the Fermi level. [26]

1.1.4.3 Quenching effect

CDs have a wide range of applications such as chemical sensing, biosensing and drug delivery. In most cases, the detection is based on changes in fluorescence

resulting from either quenching or quenching suppression [5] (Figure 9). Quenching mechanisms include:

1. Static quenching
2. Dynamic quenching
3. Energy transfer:
    - Förster resonance energy transfer (FRET)
    - Dexter energy transfer (DET)
    - Surface energy transfer (SET)
4. Photoinduced electron transfer (PET)
5. Inner filter effect (IFE)

Static quenching occurs when CDs interact with a quencher to form a non-fluorescent ground-state complex. [27]

Dynamic quenching, on the other hand, involves collisions between the quencher and CDs resulting in the return of the excited state to the ground state through energy transfer or charge transfer mechanisms. [28]

The term FRET, coined after its discovery by a German scientist in 1948, involves the transfer of photonic energy from a first fluorophore (the donor) to a second fluorophore (the acceptor), followed by emission from the acceptor. This phenomenon occurs at distances less than 10 nm between the CD and the quencher molecule. [29]

DET is based on electron transfer rather than photon transfer and requires a match in the redox potentials of the donor and acceptor. [30]

SET is a recently discovered process, commonly observed with (metal) nanoparticles, involving a metallic surface (e.g., on gold NPs) and a molecular (organic) dipole. [31]

PET is a process where an excited electron is transferred from donor to acceptor molecules, occurring at distances greater than 10 nm between the CD and the quencher molecule. [32]

IFE occurs when the absorption spectrum of the quencher in the detection system overlaps with the excitation or emission spectra of CDs. This mechanism is attributed to interactions between surface plasmons and the orbital system of a fluorophore. The IFE mechanism of CDs differs from the static and dynamic quenching mechanisms of CDs, as it does not require modification of the CDs., IFE can also occur between CDs and small metal clusters, although it is more common for quantum dots. [33]

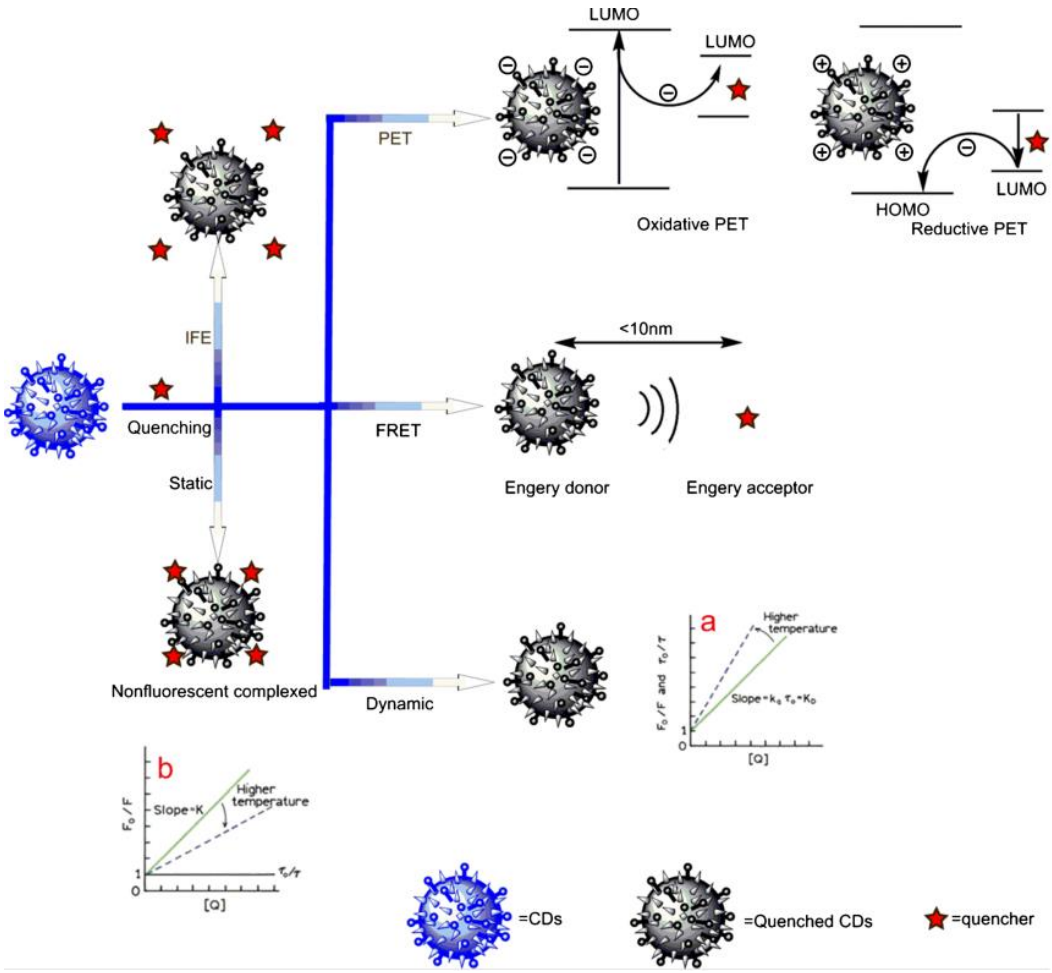

Figure 9 - Quenching mechanism. (Reproduced with permission, source [5])

1.1.4.4 Optical chirality

Chirality is the geometric property of an object that cannot be overlaid onto its mirror image. Chiral CDs (c-CDs) can be produced by utilizing chiral precursors, employing a chiral substrate, or modifying the surface of CDs with chiral molecules. The properties of c-CDs include circular dichroism and circular polarized photoluminescence. The integration of chirality and luminescence in c-CDs, makes them particularly suitable for sensing applications [34]. Chiral enantiomers exhibit optical activity due to the refractive index difference, which causes polarized light to propagate at different speeds.

c-CDs are highly selective towards cancer cells, making them effective drug carriers for tumour treatment. They can also be utilised for biosensing due to their ability to detect changes in fluorescence emission due to enantioselective interactions with analytes [35].

It is crucial to identify chiral drugs, as typically only one enantiomer is pharmacologically effective while the other may be harmful. For instance,

Levodopa is the pharmacologically active enantiomer of dopamine used for the treatment of Parkinson's disease [36].

1.1.4.5 Differences with inorganic quantum dots

Semiconductor quantum dots (QDs) have been extensively researched in recent years due to their tuneable fluorescence properties, which enable their use in bioimaging, biosensing, and theragnostic. Nevertheless, the clinical utility of these quantum dots has been significantly constrained by their inherent toxicity arising from the use of metals in their synthesis [37]. In the quest for viable alternatives, CDs have emerged as promising candidates due to their high biocompatibility, benign chemical composition, ease of functionalization, excellent physical, chemical and photochemical stability, cost-effectiveness, and straightforward synthesis still maintaining comparable fluorescence properties.

CDs and QDs have some differences in terms of fluorescence. Changes in surface functional groups have a greater impact on the fluorescence colour of CDs than modulating their size. CDs have a broader emission band compared to QDs, possibly due to their inhomogeneous chemical structure.

1.1.5 Biomedical applications

The CDs have been tested for a wide range of biological applications.

1. Chemical sensing
2. Biosensing
3. Bioimaging
4. Nanomedicine

Several intriguing applications of CDs are related to chemical sensing, especially in detecting heavy metals. The identification of heavy metals is crucial for addressing human health and environmental concerns. The detection of mercury ions (Hg^{2+}) in aqueous solutions [38], [39] and biological systems, including cells [40], was one of the first applications of CDs in this context. The fluorescence quenching mechanism is the primary method used for detecting metal ions.

CDs find applications in biosensing, particularly as fluorescent labels in immunoassays. For example, Posthuma-Trumpie et al. [41] employed carbon quantum dots (CQDs) in lateral flow and microarray immunoassays. The analytical outcomes demonstrate that CDs present a favourable alternative in terms of cost, stability, and sensitivity when compared to gold, coloured latex, silica, quantum dots, or up-converting phosphor nanoparticles.

Bu et al. [42] described an immunosensor designed for the detection of endocrine-disrupting organic pollutants. The sensor uses the FRET mechanism, where the CD-antigen system serves as a fluorescence donor.

The application of fluorescence quenching has been expanded to the detection of nucleic acids [43]. CDs have demonstrated potential as fluorescent probes for the identification of small bio-analytes, such as anti-bacterial drugs, dopamine [44], and glucose [45].

The concentration of H_2S in cells is crucial, as it acts as a signalling molecule with regulatory roles in oxidative stress and modulation of biochemical pathways. CDs are an excellent choice for fluorescent probes in H_2S detection [46], due to their ability of multi-colour emission. This unique characteristic allows clear differentiation from other tracers. Furthermore, the emission wavelength can be precisely controlled by manipulating the excitation wavelength.

As previously discussed, CDs have multiple advantages over semiconductor quantum dots that make CDs valid alternatives for bioimaging both in vitro and in vivo [47].

CDs find versatile applications in the field of nanomedicine serving as photosensitizers, radiosensitizers, and nano-carriers for drug and gene tracking and transportation. Bechet and colleagues [48] have highlighted the exceptional photosensitizing properties of CDs, which can accumulate in tumour tissues. When exposed to a specific wavelength, CDs induce the generation of oxidative species that are detrimental to tumour cells. Furthermore, CDs exhibit remarkable radiosensitizing characteristics, as documented by Andrius et al. [49]. Additionally, their fluorescence properties make them valuable in drug transport, enabling the optimization of drug administration timing and dosage. Upon reaching the target, CDs facilitate a controlled release of the drug through various mechanisms activated by pH, or photosensitive molecules attached to them [50].

1.2 CDs composites materials

1.2.1 Properties

A composite material is a substance composed of multiple phases, each possessing distinct physicochemical properties that synergistically contribute to the overall enhanced performance of the material. This unique combination results in a versatile material suitable for diverse applications. Composite materials draw inspiration from nature, such as wood and bone, to create materials with unique properties and characteristics. Cellulose fibres dispersed in a lignin phase and collagen strengthened by mineral apatite are examples of natural structures that can be replicated in composite materials.

Composite materials consist of two main phases: the matrix and the reinforcement. The matrix binds and envelops the reinforcement cohesively, forming a continuous

phase. The reinforcement, in the form of particles, fibres, or foils, imparts superior mechanical properties to the composite.

CDs are an excellent choice as a nano-inclusion in polymer matrices due to their small size and the abundance of functional groups on their surface.

The presence of the polymer contributes to the stabilization of CDs, which typically have elevated surface energy that can lead to undesirable aggregation, compromising their optical properties and sensing capabilities. Nanocomposites have demonstrated not only enhanced physical-mechanical properties but also notable swelling ability and thermal stability.

1.2.2 Preparation methods

Figure 10 illustrates the four most commonly used methods in the fabrication of composites based on CDs [51].

The first method involves preparing of CDs and support materials separately, followed by their combination. This widely adopted method preserves the stability and inherent properties of both CDs and support materials [52].

The second method involves the conjugating synthesized CDs during the polymerization of the matrix [53].

The third approach entails adding prepared support materials during the CD preparation process, enabling CDs to form directly on the support materials. This approach's success relies on the stability of the support materials or the use of moderate CD preparation conditions [54].

The fourth approach uses a one-step procedure where both precursors are simultaneously introduced [55].

In this thesis work, the chosen approach is the second one (Figure 10).

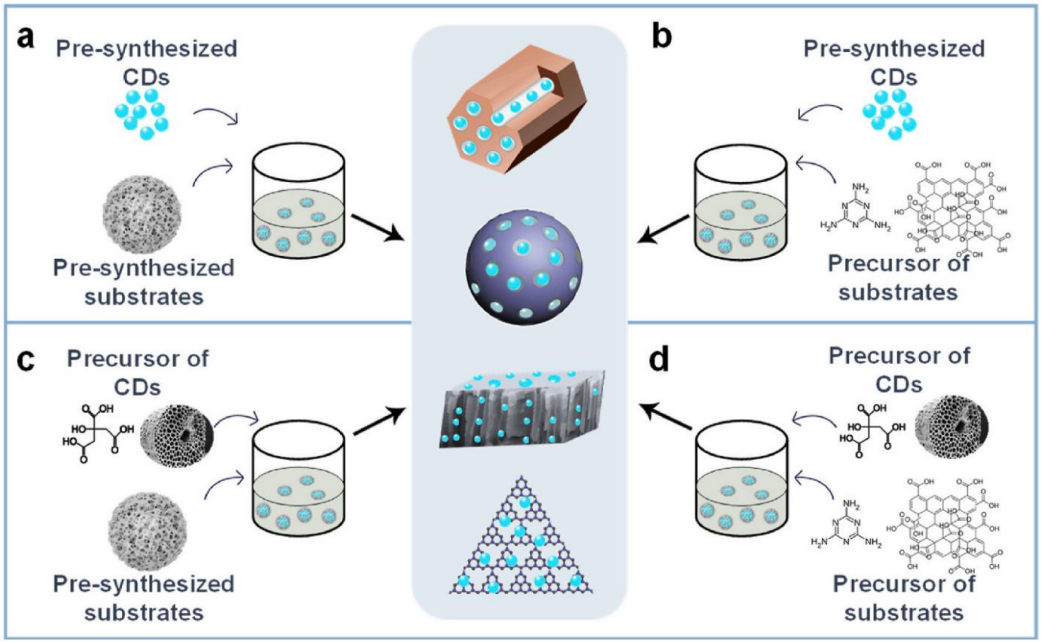

Figure 10 - CDs composites synthesis approaches (Reproduced with permission, source [51])

1.2.3 Thin films

In the biomedical field, CDs-based films have been extensively explored for various applications.

CDs exhibit significant bactericidal efficacy attributed to mechanisms such as electrostatic repulsion, physical penetration, and oxidative stress. Zang et al. [56] demonstrated that membranes modified with GOQDs exhibit antibacterial and antibiofouling effects against Escherichia coli (*E. coli*) and Staphylococcus aureus (*S. aureus*).

Films that incorporate CDs are highly effective in detecting fungal spores in the surrounding environment [57]. The fluorescence quenching process upon interaction with spores is a reliable detection method. These films are known for their stability, exceptional sensitivity, and rapid response times, making them ideal sensors for clinical, microbiological, and tissue engineering applications [57].

CDs-based films present a promising alternative to commercial enzymatic amperometric devices for glucose sensing in the context of biomedical applications. Monitoring glucose levels in the human body stands as a crucial indicator of a patient's health status, and it requires continuous exploration of sensors that offer heightened specificity and user-friendliness. Fluorescence-based systems are advantageous due to their high selectivity, minimal invasiveness, and the ability to capture biomolecules through mechanisms like FRET or fluorescence quenching. CDs serve as excellent fluorophore probes to reflect glucose levels (Figure 11) [58].

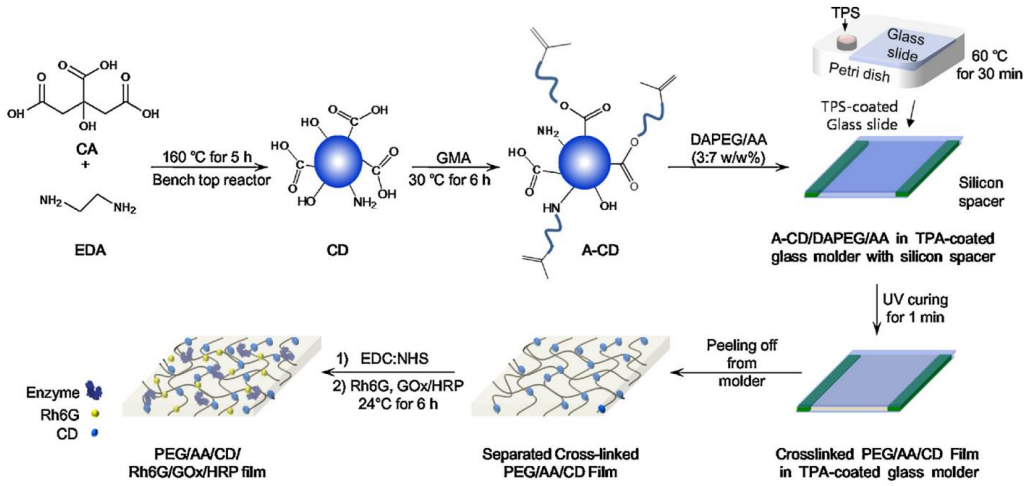

Figure 11 - Schematic illustration of CDs-based films syntethis for glucose sensing. (Reproduced with permission, source [58])

1.3 Polymers

1.3.1 Classification

Polymers are large molecules composed of small repeating units called monomers. As a highly variable and versatile material class, there are different criteria for their classification which mainly are:

1. Mechanism of polymerization
2. Molecular structure
3. Origin of the polymer
4. Thermal properties
5. Repetitive units

The classification based on the mechanisms of polymerization establishes two types of polymers: addition polymers and condensation polymers. Addition polymers (e.g. poly(ethylene), poly(propylene)) are formed by the recurrent addition of monomers without the formation of waste products (e.g. poly(ethylene), poly(propylene)). Condensation polymers, on the other hand, are produced through a process that involves the removal of small molecules, such as water or alcohol, at each step of monomer addition.

The second classification based on the polymer structure leads to categorise the polymers as linear, branched, or cross-linked. Linear polymers have a simple, unbranched structure, while branched polymers have side chains prolonging from the primary chain. Cross-linked polymers form interconnected chains, creating a three-dimensional network that imparts enhanced strength and stability.

The classification based on the origin distinguishes the polymers either natural or synthetic or artificial. Natural polymers (e.g. proteins, DNA) derive from biological

sources, while synthetic polymers (e.g. PVC, nylon) are man-made. Artificial polymers can include both synthetic and natural ones that have been modified to enhance their properties or performance.

The thermal properties enable to distinguish thermoplastic and thermosetting polymers. The thermoplastics are non-crosslinked and can be melted and re-shaped several times. The thermosetting polymers are highly crosslinked, maintain their shape once hardened and undergo degradation if melted again.

Monomers that are monofunctional, result in a thermoplastic material. The chains in this system are linear or poorly branched and interact with each other through secondary bonds (hydrogen bonds, Wan Der Waals forces). On the other hand, multifunctional systems produce thermosetting polymers. In this case chains are linked to each other by chemical bonds, making the material infusible and insoluble. This chemical bonding process ensures that the material retains its shape and strength even under high temperatures and pressure.

Considering the *repetitive unit*, it is possible to differentiate homopolymers which are composed of identical repeating monomers, and copolymers which incorporate two or more types of monomers in their chains.

Additional classifications can be based on factors such as the biodegradability *in vivo*, in relation to the homogeneity of the molecular weight, to the stereochemical structure or to the molecular weight.

1.3.2 Polymers for biomedical applications

Biomedical polymers have been extensively developed for promising applications in various biomedical domains. These include smart drug delivery, disease detection and diagnosis, biosensing, regenerative medicine, and disease treatment (Figure 12) [59].

Polymers derived from natural sources like proteins (e.g., silk, collagen, soy, fibrin gels), polysaccharides (e.g., chitin/ chitosan, alginate, and hyaluronic acid derivatives), and polynucleotides (e.g., DNA and RNA) are predominantly biodegradable and interact favourably with the biological environment. However, their mechanical properties are often limited, and degradation tends to be uncontrolled. In contrast, synthetic polymers (e.g. (PEG), poly(caprolactone) (PCL), or poly(lactic-co-glycolic acid) (PLGA)) offer the advantage of controllability in terms of composition, structure, mechanical properties, and degradation, despite their lack of inherent bioactivity [60].

In biomedical applications, polymers are categorized as either biodegradable or non-biodegradable. The choice between these categories depends on the specific requirements of the application at hand [60].

Non-biodegradable polymers, such as PEG and Ultra High Molecular Weight Poly-Ethylene (UHMWPE), are commonly used permanent implantable prostheses or as substitutes for entire damaged tissues or organs.

Biodegradable polymers are the preferred choice for temporary biomedical applications, such as controlled delivery systems, temporary scaffolds for cell culture and tissue regeneration, and absorbable devices for wound closure. Noable examples of biodegradable polymers include poly(lactic acid) (PLA), PCL, and gelatine methacrylate (gelMA). These polymers degrade, metabolize, and excrete from the body after fulfilling their support or delivery function, without causing any toxic side effects [60].

When selecting polymers for biomedical applications, it is crucial to prioritize biocompatibility and biodegradability. Investigating biocompatibility is essential to ensure that the device can establish contact with the biological environment without causing inflammation, rejection, infection, tissue damage, systemic reactions, or compromising its functionality [60].

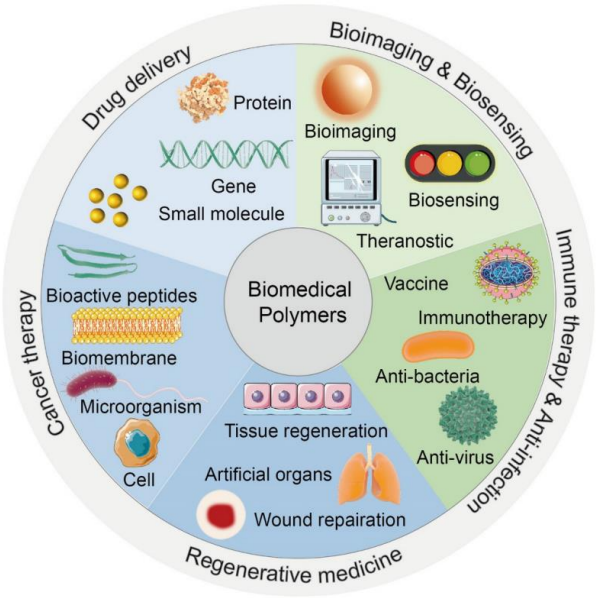

Figure 12 - Application of biomedical polymers (Reproduced with permission, source [59])

1.3.3 Photopolymerization

Photopolymerization is an addition polymerization mechanism that uses the energy derived from various forms of radiation (UV rays, IR, visible light, γ rays and electron beams) to initiate the reaction. Photopolymerization is possible only in presence of molecules capable of absorbing radiation and generating reactive species that can initiate the polymerization reaction. The reactive species can be radicals, cations, or anions [61].

1.3.3.1 Photopolymerization by radical addition

Figure 13 illustrates the mechanism of photopolymerization by radical addition. A radical photopolymerization reaction is usually divided into three phases: initiation, propagation, and termination. The first phase is the **initiation** in which the initiator (I) absorbs light (*hv*) and generates the radical monomers (R·). The radicals react with the monomer/pre-polymer (M) to produce the radical polymer (P·). The second phase is **propagation** in which the P· react with other monomers increasing the molecular weight of the chains. **Termination** occurs in the third phase through two mechanisms: two polymer chains interact with each other instead of with new monomers (P·–P·), or a transfer of hydrogen atoms may occur if a fast-reacting radical interacts with a slower-reacting radical, leading to the termination of the process [62].

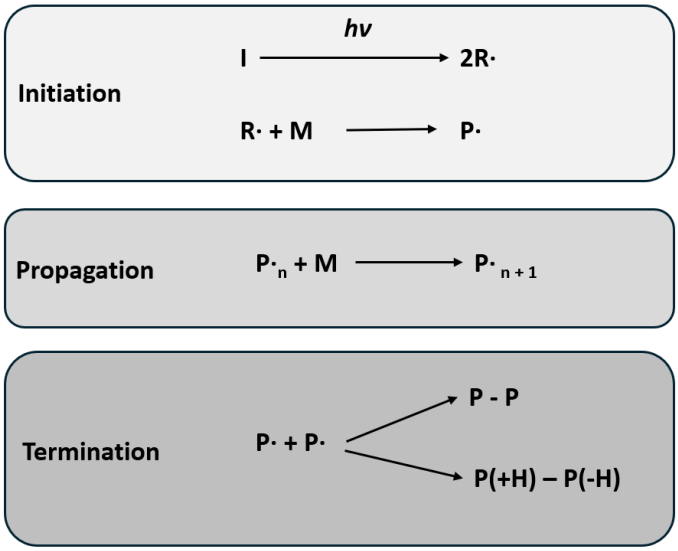

Figure 13 - Steps of photopolymerization.

The intensity of the radiation varies along the thickness of the formulation. In fact, there is a gradient of intensity which decreases with the increase of the distance from the surface. This gradient significantly affects the conversion of reactive groups, resulting in non-uniform polymerization throughout the material.

1.3.3.2 Photoinitiation mechanism

The absorption spectrum of the photoinitiator must be compatible with the emission spectrum of the source of radiation. Typically, UV or visible light is utilized, ensuring safety in the presence of biological compounds such as cells [63]. The photoinitiator should also possess good solubility and stability, high reactivity, and not affect the final properties of the polymerised material [64].

Typically, a photoinitiator is an organic molecule. When exposed to light, the molecule transits from its ground state to an excited singlet state (S1). The electron elevated to the excited state retains its original electronic spin (Figure 15).

The singlet state transits to a triplet state (T1) through an intersystem conversion, involving a reversal of electronic spin. The triplet state then progresses, leading to the formation of radicals that initiate polymerization [64] (Figure 15).

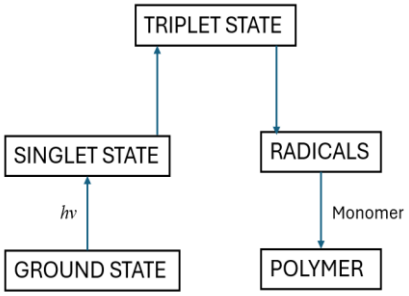

Figure 15 - Stages of the evolution of the initiator molecule after the absorption of energy by radiation.

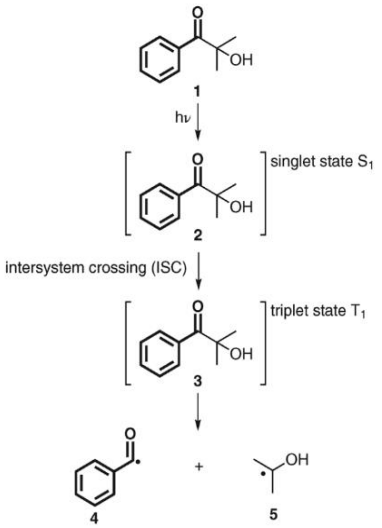

Figure 14 - mechanism of radical generation with Norrish type I mechanism of a hydroxyphenylketone.

The molecule transits from a triplet state to a radical state through either cleavage (Norrish I-type mechanism) or hydrogen extraction (Norrish II-type mechanism) [65]. This thesis work employs a Norrish I photoinitiator. Norrish I photoinitiators, when excited by light radiation, undergo homolytic cleavage, producing two radicals. Hydroxyphenylketones act as Norrish I-type initiators (Figure 14).

Materials that can be photocured must have active functional groups. Radically polymerisable resins are often based on the highly reactive (meth)acrylate functionalities (e.g. poly(ethylene glycol)methacrylate). As shown in Figure 16, other functionalities can also be used such as polyester, vinyl, vinyl ether, thio-ene/yne and even cationic based systems [66].

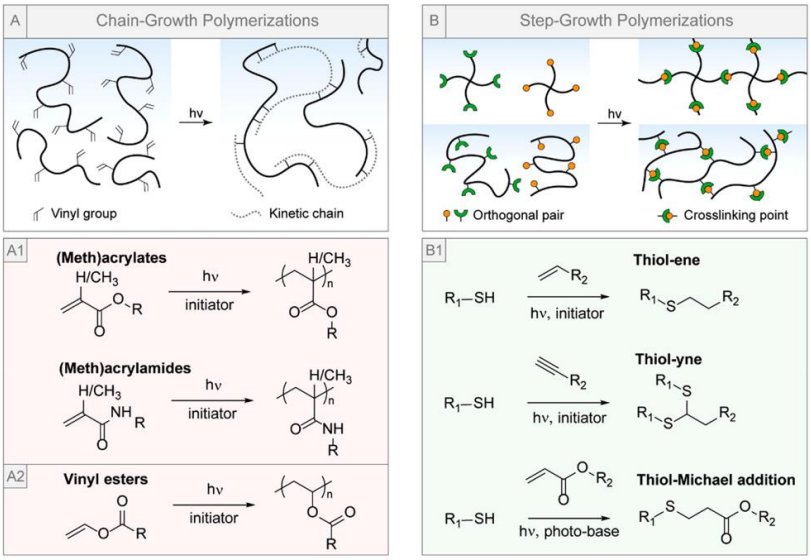

Figure 16 – Examples of functionalities. (Reproduced with permission, source [66])

2 Aim of the work

The aim of this thesis work is the preparation and characterization of a composite thin film made of PEGMEMA and CDs synthetised from CA and p-DPA.

The films obtained could be used either to monitor interfaces for biomedical applications (Figure 17, 1) or to release active substances/CDs (Figure 17, 2) or a combination of the previous ones. In each case the main source of information is the variation of photoluminescence (PL) intensity throughout the film life cycle.

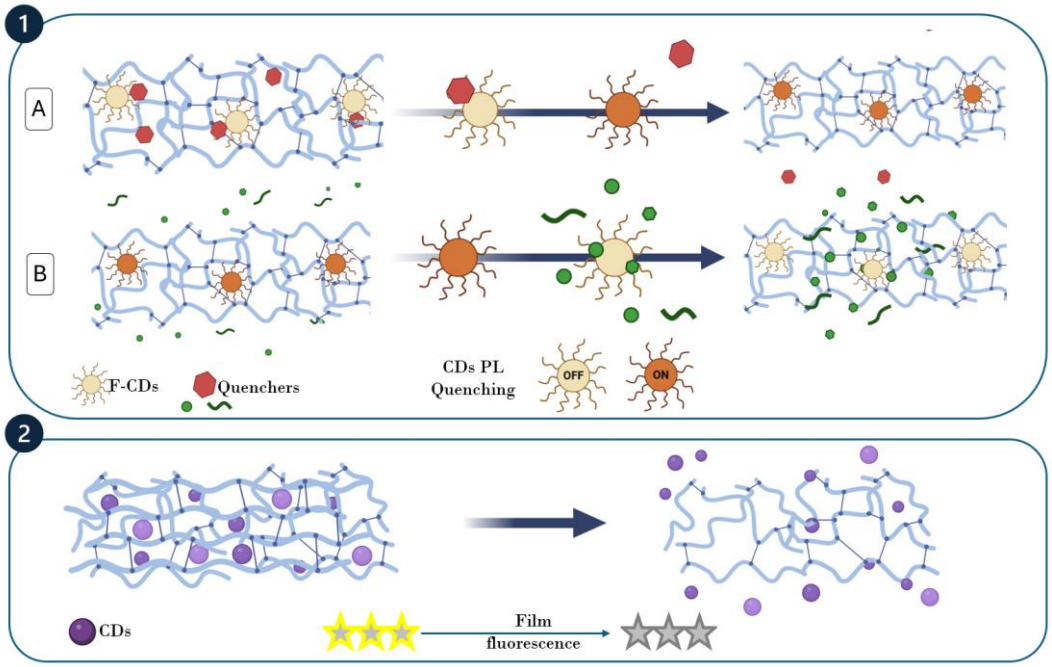

Figure 17 - Graphical abstract.

3 Materials and methods

3.1 Materials

The following reagents were used for the synthesis of CDs: Citric Acid (CA) purchased from Nortembio, 1,4-Phenylenediamine (p-DPA) purchased from Fluka, Deionized water (DW).

The following reagents were used for the functionalization of CDs: 2,3-Epoxypropyl methacrylate (EPM) purchased from Sigma-Aldrich, Petroleum ether purchased from Carlo Erba Reagents.

The following reagents were used for the photopolymerization of CDs-based films: 2-Hydroxy-2-methylpropiophenone (PhI) purchased from Sigma-Aldrich, Poly(ethylene glycol) methyl ether methacrylate (PEGMEMA) purchased from Sigma-Aldrich.

3.2 Methods

3.2.1 Synthesis of CDs

Five solutions containing CA and p-DPA in different molar ratios (Table 1) were used to prepare CDs (Figure 18, step 1). An analytical balance of Radwag was used to weight the reagents. Each solution was sonicated for 1 h at 450 W alternating ON (20s) and OFF (10s) phases to avoid excessive heating (Figure 18, step 2). A Vibra Cell sonicator purchased from Sonics was used to synthesize the CDs. The purple-coloured solution resulting from sonication was then purified by dialysis.

Table 1 – Quantities of materials used for the syntheses for each molar ratio.

Molar ratio CA/p-DPA	CA (g)	p-DPA (g)	DW (ml)
3:1	1.01	0.19	20
3:2	1.01	0.38	20
1:1	1.01	0.57	20
2:3	1.01	0.84	20
1:3	1.01	1.73	20

3.2.2 Purification of CDs

Purification was performed by placing each solution in a dialysis membrane purchased from Real laboratory supplies with cut-off value of 1000 MW (Figure 18, step 3). The dialysis allows to refine the molecular weight and size distribution of the CDs. The membranes were agitated in water for 72 h using a VELP Scientifica magnetic multistirrer. The water was changed every 24 h. The content of the membrane was collected, and oven dried at 80°C until complete evaporation of the water (Figure 18, step 4).

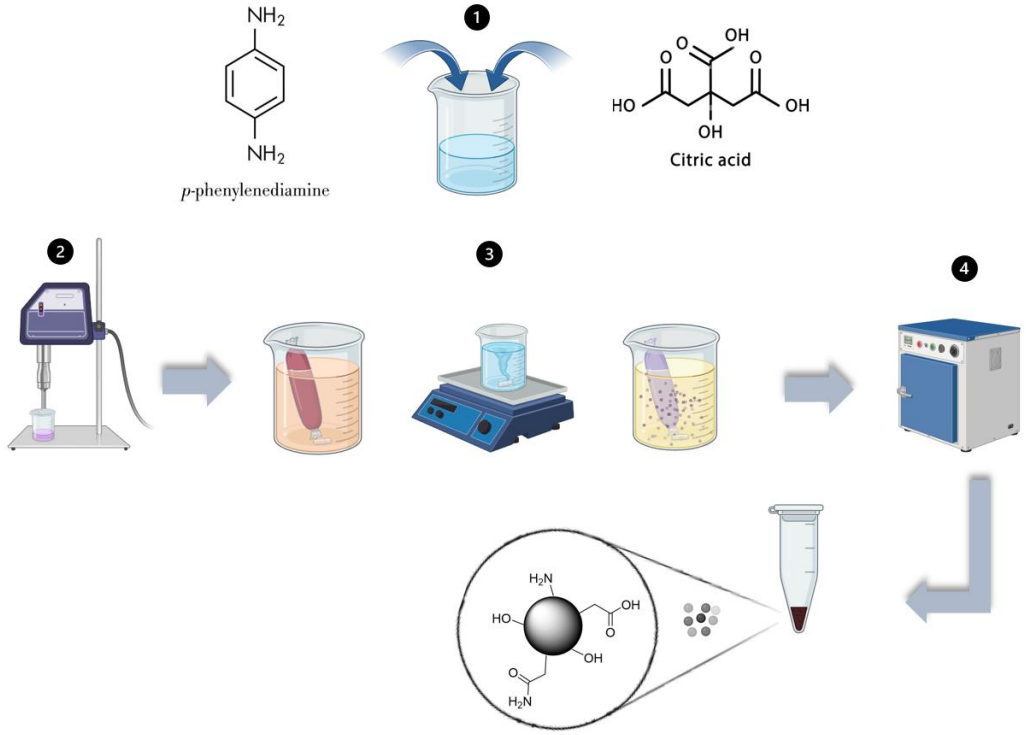

Figure 18 - Steps of the synthesis of CDs.

3.2.3 Characterization of CDs

3.2.3.1 Fluorometer analysis

Fluorometer analyses were repeated for each CA/p-DPA molar ratio CDs.

The first analysis conducted was a fluorometer analysis. Characterising CDs from a fluorescence point of view is crucial for their applications. For the analysis, a solution of CDs in a concentration of 0.1 mg/mL was produced with the help of an Elma sonicator bath. Once a solution with well-dispersed CDs was obtained, it was poured inside the Hellma quartz cuvette and placed in the PerkinElmer LS-55 fluorometer.

It was decided to excite the sample with 8 wavelengths between 240 nm and 310 nm in increments of 10 nm. The beam bandwidth was set at 5 nm, while scan speed 50 nm/s, for higher resolution.

The data obtained were used to plot graphs of the emission intensity (arb. un.) as a function of the wavelength (nm). The data had to be reprocessed to eliminate overtones produced by optical interference or background noise which could affect the measurement of the fluorescence spectrum. A strong overtone over 500 nm affects the observation of the significative emission peaks between 300 and 500 nm for all excitation wavelengths. Overtones were eliminated by cutting the signal outside the range of interest as shown in (Figure 23).

3.2.3.2 FT-IR spectroscopy

FT-IR spectroscopy was repeated for each CA/p-DPA molar ratio CDs.

Nicolet 5700 Fourier-transform infrared spectrometer from Thermo Fisher Scientific was used for FT-IR spectroscopy. The acquisition number chosen for spectrum sampling was 64 and the wavelength range selected was 500 cm^{-1} to 4000 cm^{-1}.

Before proceeding to the acquisition of the spectra of the CDs, the spectrum of the air in the laboratory was collected as background. Subsequently, the background was subtracted from the spectra of the CDs.

3.2.3.3 AFM analysis

AFM analyses were conducted only for (3:1) and (2:3) CDs. AFM characterizations have been performed in tapping mode with a Bruker Innova® Atomic Force Microscope to monitor the dimension of CDs. Budget Sensors TAP300AL-G tapping mode probe with tip apical diameter <10 nm was used. The maps shown in the following were acquired using a scan rate of 0.5 Hz in ambient conditions. Gwyddion software was employed for image analysis.

The samples were prepared by solubilising by sonication the CDs in DW with a concentration of 0.1 mg/mL. Drops were then taken from each solution and deposited on a silicon wafer purchased from Shin Etsu. Two consecutive depositions were made in the same spot to increase the concentration of CDs on the substrate. For the analysis, it was decided to place the cantilever on the droplet's coffee ring to be sure of finding a sufficient concentration of CDs.

3.2.3.4 Thermogravimetrical analysis TGA

TGA analyses were performed using a Netzsch TG 209 F3 Tarsus thermo-microbalance while heating under a nitrogen flow of 40 ml/min from 40 to 800 °C at a rate of 20 °C/min.

3.2.3.5 UV/VIS

UV-VIS absorbance was measured with a PerkinElmer Lambda 35 UV/VIS Spectrometer. The analysis was performed for wavelengths ranging from 300 nm

to 750 nm. The mass extinction coefficient ε_λ has been calculated through the Lambert-Beer law,

$$A = \varepsilon_\lambda \, l \, \rho \qquad \text{(Eq. 1)}$$

where A is the absorbance, l is the optical path and ρ is the mass concentration. The solutions to be analysed have a 1 mg/mL concentration of CDs.

3.2.4 Carbon dots functionalization

Functionalisation was conducted only for (2:3) CDs.

The CDs were functionalised following the protocol of M. J. Cho et al. [43]. The aim was to make CDs with exposed acrylic groups which were exploited for the subsequent photopolymerization. EPM reacted with the functional groups exposed on CDs and created a shell of acrylic groups.

A sonicated aqueous solution of CDs with a concentration of 5 mg/mL was prepared. 5 mL of CDs solution was combined with 0.3 mL of EPM (Figure 19, step 1). The resulting solution was kept stirring for 6 h at room temperature on a magnetic stirrer (Figure 19, step 2). The solution after 6h assumed a biphasic form then a petroleum ether wash was performed using a separatory funnel with a retort stand. The phase containing functionalised CDs (F-CDs) was recovered and unreacted substances removed (Figure 19, step 3,4). The recovered aqueous solution was oven dried (Figure 19, step 5).

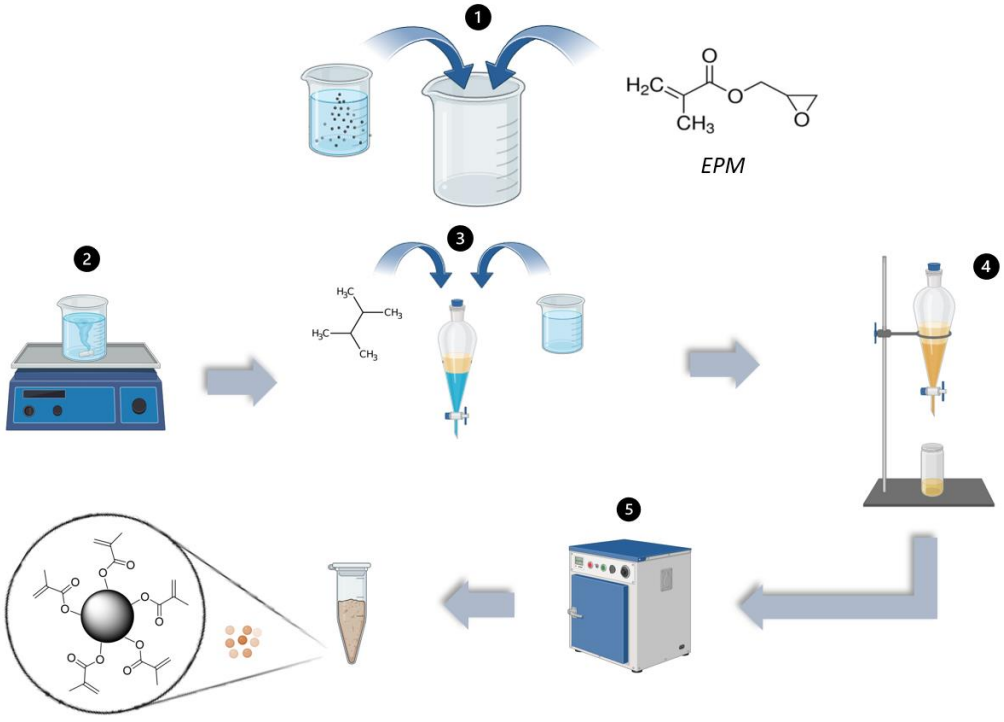

Figure 19 - Steps of the functionalization of CDs.

3.2.5 Composite preparation

A stock solution with the polymer and the PhI (2% wt) was prepared (Figure 20, step 1). The stock solution was used to prepare 4 solutions with different concentrations of F-CDs (Table 2), a solution with (2:3) CDs, a solution with (3:1) CDs and the blank (Figure 20, step 2). The solutions containing the CDs were sonicated for about 1 h all the resulting solutions were deposited by drop casting on glass laboratory slides (Figure 20, step 3), creating a layer about 1 mm thick (0.1 ml of solution).

Photopolymerization took place under a fume hood, using a HAMAMATSU Spot UV light source (Power 4500 mW/cm^2). It was placed one slide at a time in a quartz chamber. Nitrogen was run through the chamber to maintain an inert environment and prevent oxidation of the sample on the surface (Figure 20, step 4).

Table 2 - CDs, PhI and Ph-polymer quantities for each sample.

CDs	CDs (%wt)	Polymer (%wt)	PhI (%wt)
F-CDs	4.8	93.2	2
F-CDs	2.9	95.1	2
F-CDs	1.0	97.0	2
F-CDs	0.5	97.5	2
(2:3) CDs	1.9	96.1	2
Blank	0	98.0	2

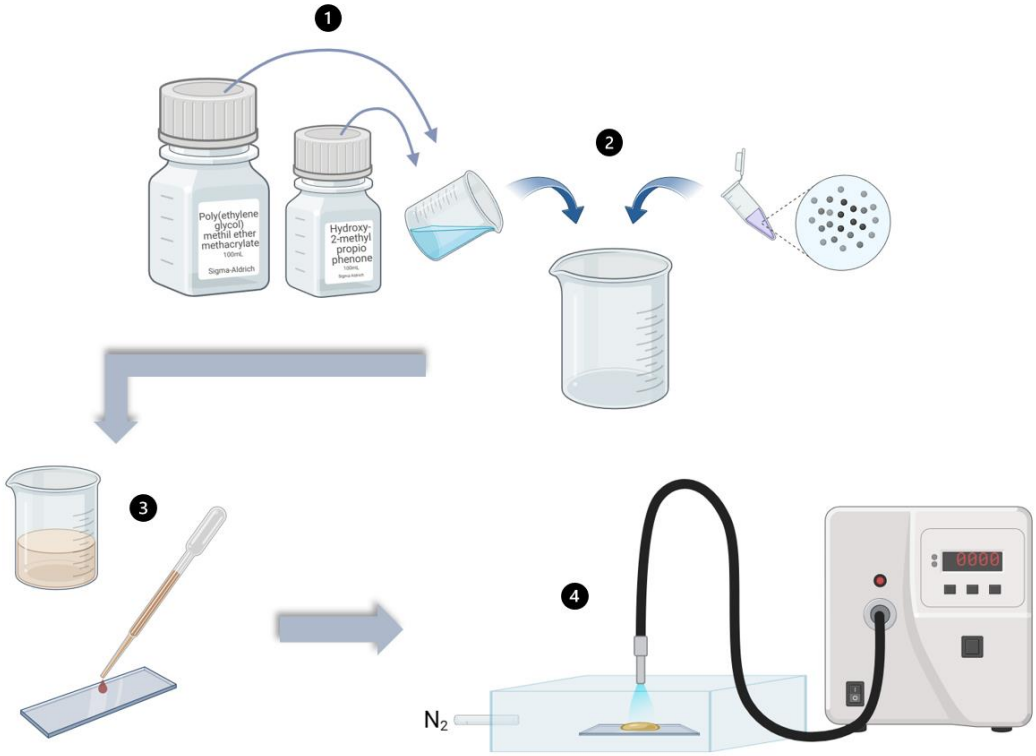

Figure 20 - Steps of composite film preparation.

3.2.6 Composite characterization

3.2.6.1 Fluorometer analysis

The fluorometric analysis of the films was conducted by placing the slides in the fluorometer on the slide holder. It was decided to excite the sample with 8 wavelengths between 240 nm and 310 nm in increments of 10 nm. The entrance and exit slits were set at 5 nm, while scan speed was set at 50 nm/s, for higher resolution.

3.2.6.2 TGA

TGA analysis of each type of CDs was performed using a Netzsch TG 209 F3 Tarsus thermo-microbalance while heating under a nitrogen flow of 40 ml/min from 40 to 800°C at a rate of 20 °C/min.

3.2.6.3 Swelling test

The films chosen for swelling test were the one without CDs, the one with non-functionalised CDs and the one with F-CDs (4.8%). The films were kept in DW for 7 days. After 7 days the films were kept for 24 h exposed to the air and then analysed by fluorometer to evaluate the CDs release after the swelling of the films. The films were weighed before and after swelling.

4 Results and discussion

4.1 Carbon dots

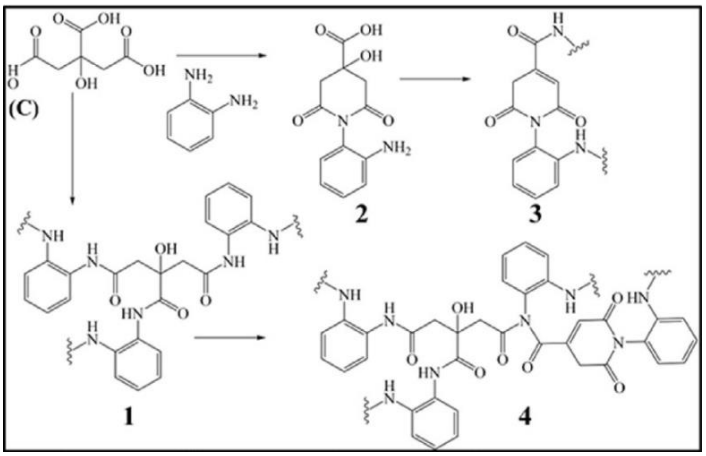

Figure 21 - Possible mechanisms of reaction of CA and p-DPA. (Reproduced with permission, source [10])

The high-intensity ultrasound produced by the sonicator develops spots at high temperature and pressure where aromatic amine heterocyclization takes place. One possible reaction is the formation of amide derivatives. The amidation of the carboxylic groups of CA with the amine groups of DPA leads to the formation of random cross-linked polymeric structures (Figure 21, 1).

The carboxylic groups of CA provide many unsaturated carbons that favour coupling with other molecules via π-bonds. The reaction of the amine groups of DPA constitute two structure growth points. The amine groups can react either with amine groups of another DPA molecule or with the carboxylic groups of CA to form an unsaturated cyclic amine (Figure 21, 2-3), with functionalities such as carboxylic groups and PDA residue.

The hydroxyl groups of CA favour the formation of heterocyclic structures containing nitrogen atoms. Heterocyclic structures can react with carboxyl groups to form a more complex structure (Figure 21, 4).

The CDs resulting from this synthesis are cross-linked heterocyclic structures containing N atoms. The structures formed are organised in parallel planes with external functional groups.

4.2 Characterization of CDs

4.2.1 Fluorescence Spectroscopy

The analysis at the fluorometer was the first one conducted and allowed the selection of the optimal synthesis molar ratio considering the fluorescence intensity. The analyses showed that CDs with a 3:1 AC-DPA molar ratio has a higher fluorescence intensity than the others (Figure 23, A-E).

The emission with a 3:1 AC-DPA is excitation dependent, and the fluorescence peaks are centred at 355 nm with an intensity maximum corresponding to excitation at 240 nm (Figure 23, A). The synthesis with 3:1 CA-DPA was preliminarily selected to be scaled up due to the highest fluorescence intensity. Also, the emission for the other molar ratios is excitation dependent (Figure 22).

3:1 ratio has two excitation-dependent energy bands (Figure 22, A). 3:2 ratio has two excitation-dependent energy bands (Figure 22, B). 1:1 CDs has three excitation-dependent energy bands (Figure 22, C). 1:3 ratio has two excitation-dependent energy bands (Figure 22, D). 2:3 ratio has two excitation-dependent energy bands (Figure 22, E).

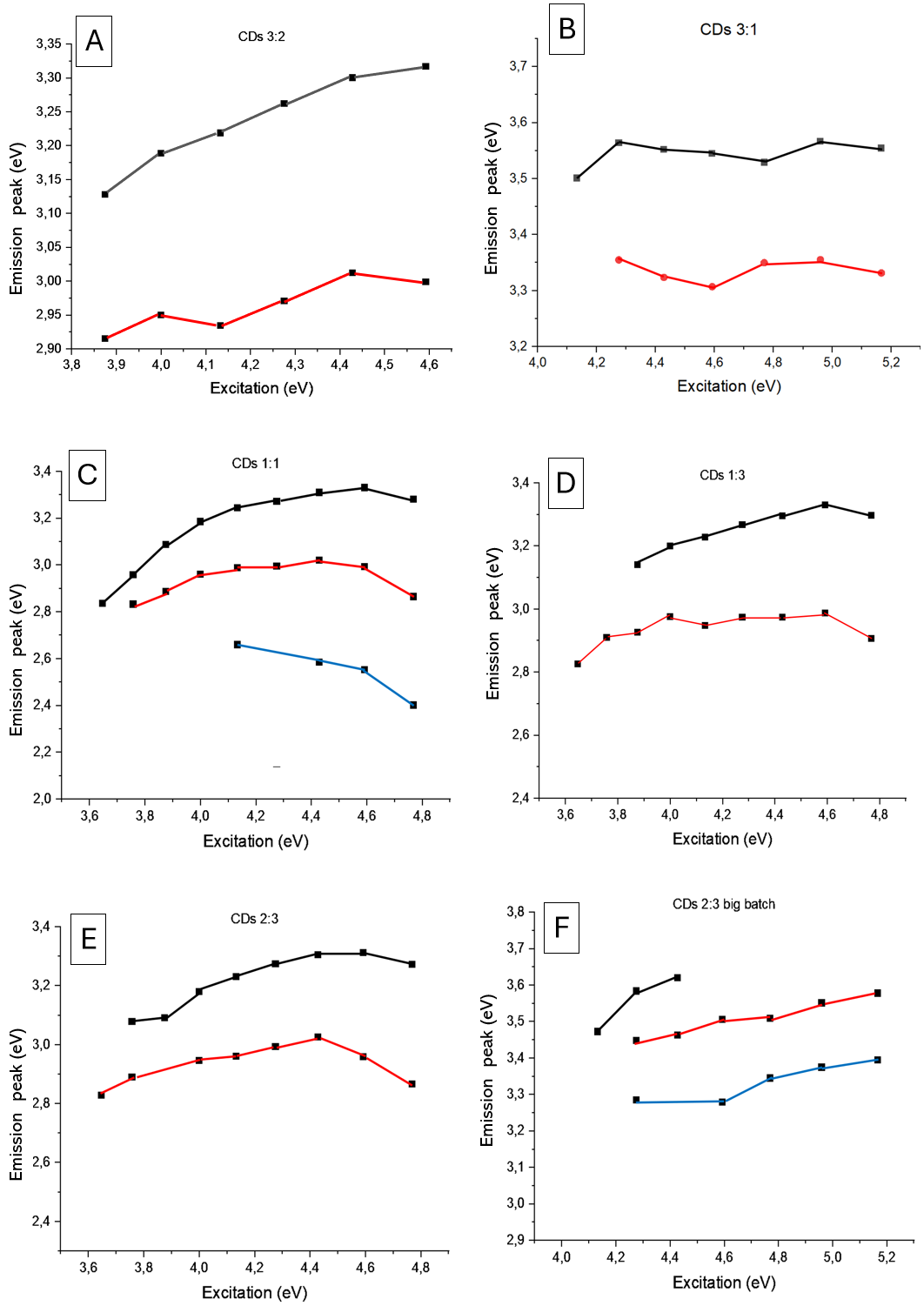

Figure 22 - Emission energy peak vs graphs Excitation energy for CDs.

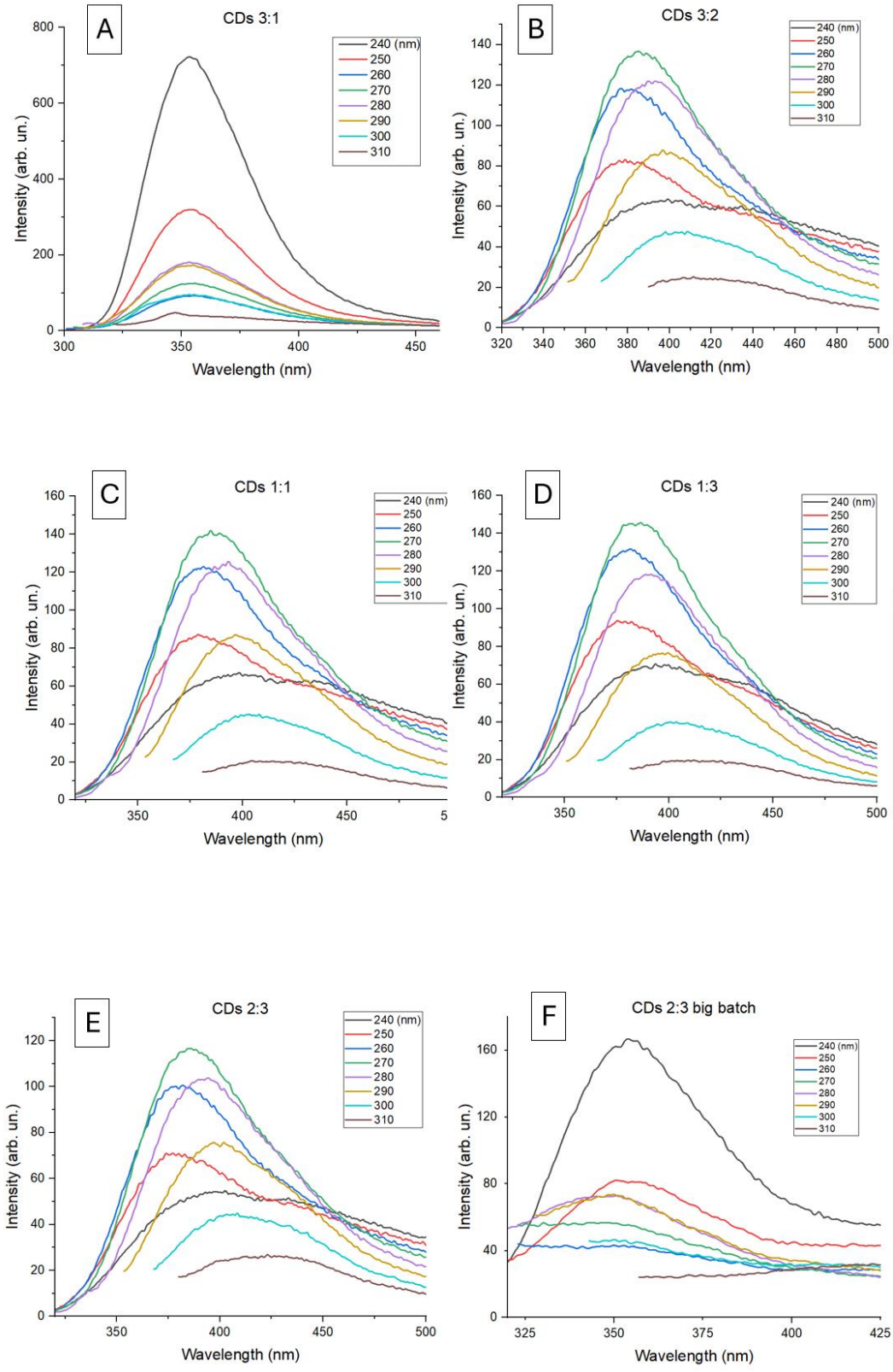

Figure 23 - Fluorescence spectra of CDs.

At high concentrations of CA, CA decarboxylates to form CO_2, while DPA tends to polymerise with itself by not finding the free carboxyl groups. A polyaniline with AC pendants is obtained.

Among the molar ratios, the 2:3 AC-DPA allowed the production of more CDs in less time. The fluorescence intensity of the 2:3 AC-DPA CDs synthesised from larger amounts of precursors was comparable with the one of the initial syntheses.

Some differences can be seen between the fluorescence spectra of the small batch and the big batch of 2:3 CA-DPA CDs. For the initial synthesis, the highest intensity emission peak is centred at 386 nm and is due to excitation at 270 nm. For the larger batch the highest fluorescence peak is centred at 355 nm and is due to excitation at 240 nm. With excitation at 240 nm, the emission peak has twice the intensity of the other peaks. Furthermore, the emission is still excitation dependent (Figure 23, E-F).

Due to high fluorescence intensity and productivity, functionalisation (Figure 24) and subsequent analyses were conducted on the 2:3 CA-DPA CDs.

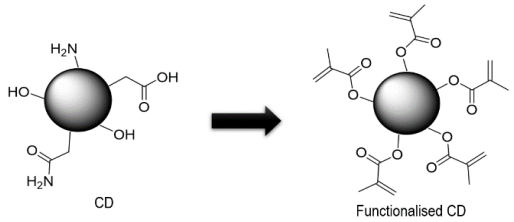

Figure 24 - CDs functionalisation.

The fluorescence spectrum of the F-CDs is excitation independent. The intensity peaks are 3 times higher than the non-functionalised CDs and centred at 445 nm. The distance between the peaks decreases as the excitation frequency increases (Figure 25, A). Comparing the normalised fluorescence maxima for non-functionalised and functionalised CDs shows a redshift of the emission peak (Figure 25, B) due to the presence of the double bonds on the surface (Figure 24). Also, the emission for the F-CDs is excitation dependent (Figure 26).

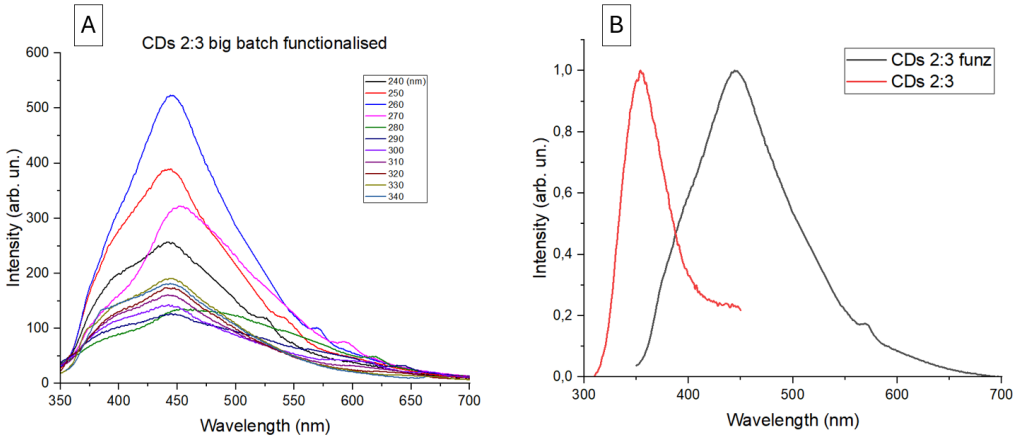

Figure 25 - Fluorescence spectra.

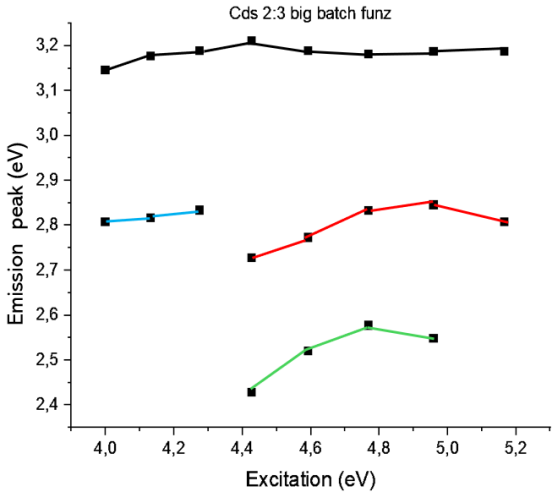

Figure 26 - Emission peak energy vs Excitation energy graphs for F-CDs.

4.2.2 FT-IR Spectroscopy

Through FT-IR spectroscopy of CDs, it is possible to identify absorption bands related to bending and stretching of bonds. It is possible to understand the growth mechanisms of CDs and obtain information about the final structure by observing the spectra of the precursors. Figure 27 shows the IR spectra of CA, p-DPA, 2:3 CDs and F-CDs.

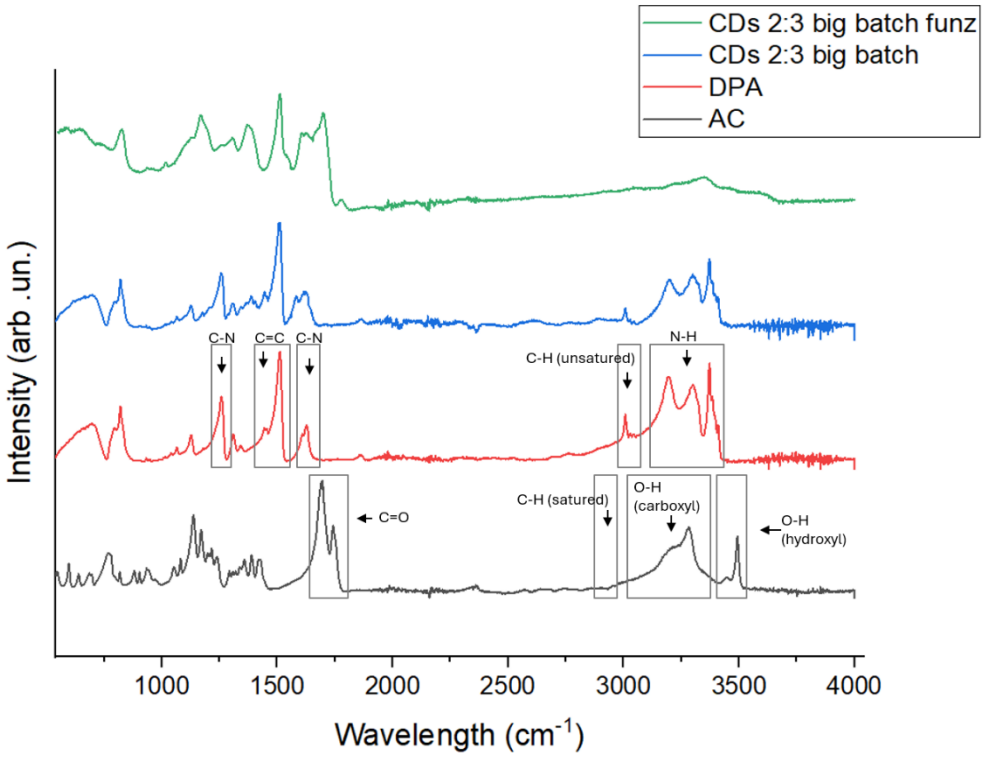

Figure 27 - FTIR spectra of CA, p-DPA, CDs (2:3) and F-CDs.

In the CA spectrum there is a peak at 3500 cm^{-1} due to the hydroxyl groups OH and a band between 3000 and 3500 cm^{-1} due to the hydroxyls of the carboxylic acids

COOH or the alcohols COH. The shoulder to the left of the OH peak indicates that it is possible to form bonds with both another OH and a COOH. The broad band of OH carboxyl groups is the combination of three different peaks due to the three carboxyl groups of CA. The heights of the peaks are related to the way the three carboxyl groups of the CA molecules interact with each other. The peak between 2750 and 2950 cm^{-1} is related to the saturated CH groups (sp3 C). In the region between 1680 and 1800 cm^{-1} there are two intense peaks due to the stretching of C=O bond that confirm the presence of carboxylic acid.

In the spectrum of DPA, there are peaks between 3200 and 3400 cm^{-1} due to N-H bonds. The three peaks from the lowest to the highest energies correspond to primary, secondary and tertiary amines. Around 2950 $cm^{-1,}$ there is a peak usually found in the aromatic groups due to the unsaturated C-H bond (sp3 C). Compared to the saturated C-H peak in the CA spectrum, this peak is higher due to the high polarity. At about 1660 cm^{-1} there is a very intense peak due to the stretching of the carbon double-bonded to another carbon (C=C) in an aromatic ring. Between 1490 and 1540 cm^{-1} there is the C-N bending signal. This is important because as DPA quantity increases, the band grows. The aromatisation band provides information on the amount of DPA in the compound.

Comparing the spectrum of CDs with that of CA, the OH peak at 3500 cm^{-1} disappears because CA has reacted with DPA. The peak due to the saturated C-H group becomes less intense due to the formation of aromatic structures. The peak due to the C=O of the free carboxyl groups disappears because of the reaction with the amine groups of DPA.

Comparing the spectrum of CDs with that of DPA, the peaks related to the N-H bond change in intensity due to the reactions between the amine groups of DPA and the carboxyl groups of CA that give rise to the amides. Between 1600-1680 cm^{-1} there is a peak splitting due to the insertion of atoms in the aromatic structures causing a shift in the aromatic ring band towards lower wave numbers.

Figure 29 shows that varying the CA-DPA molar ratio, the spectra vary. The diversity is due to the different structures formed through the amidation reaction of the carboxyl groups of CA with the amine groups of DPA and through the condensation reactions of CA itself and DPA. The signals related to the aromatic part (1600-1680 cm^{-1}) increase when there is more DPA in the CDs. The fragments that constitute the polymer structure of CDs with more DPA are more similar to the starting DPA and less to CA or its derivatives (amides). Sometimes, when there is a lot of CA, the latter tends to break down and does not make amides but radical reactions that directly connect two DPAs.

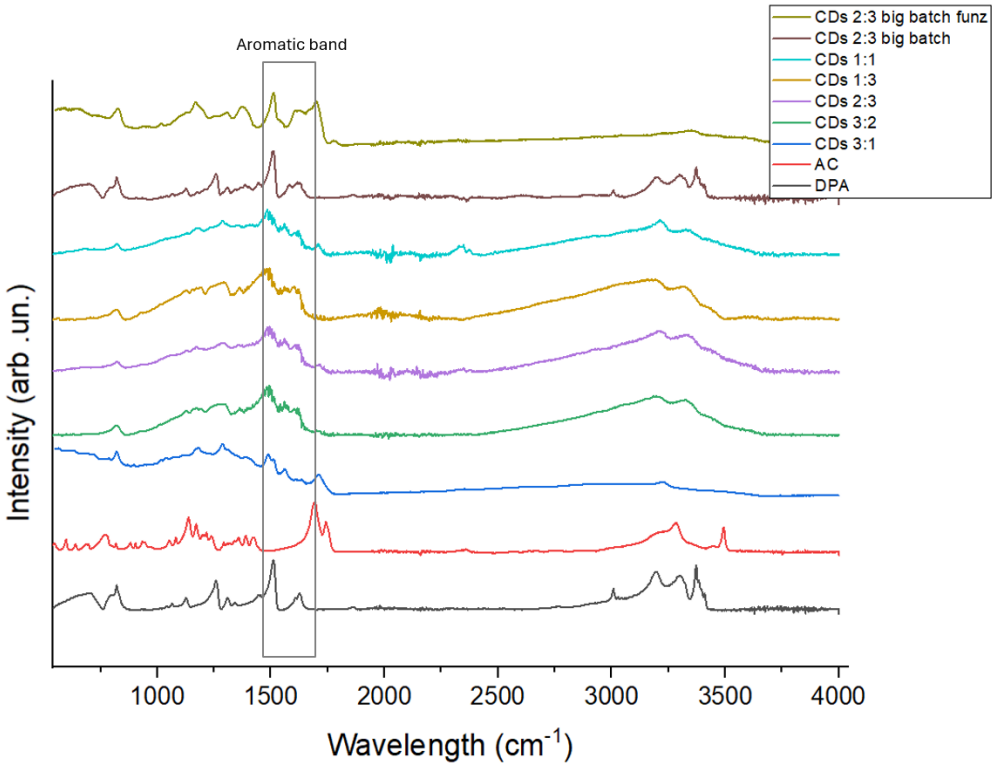

Figure 29 - Comparison of FTIR spectra of CDs with different molar ratios.

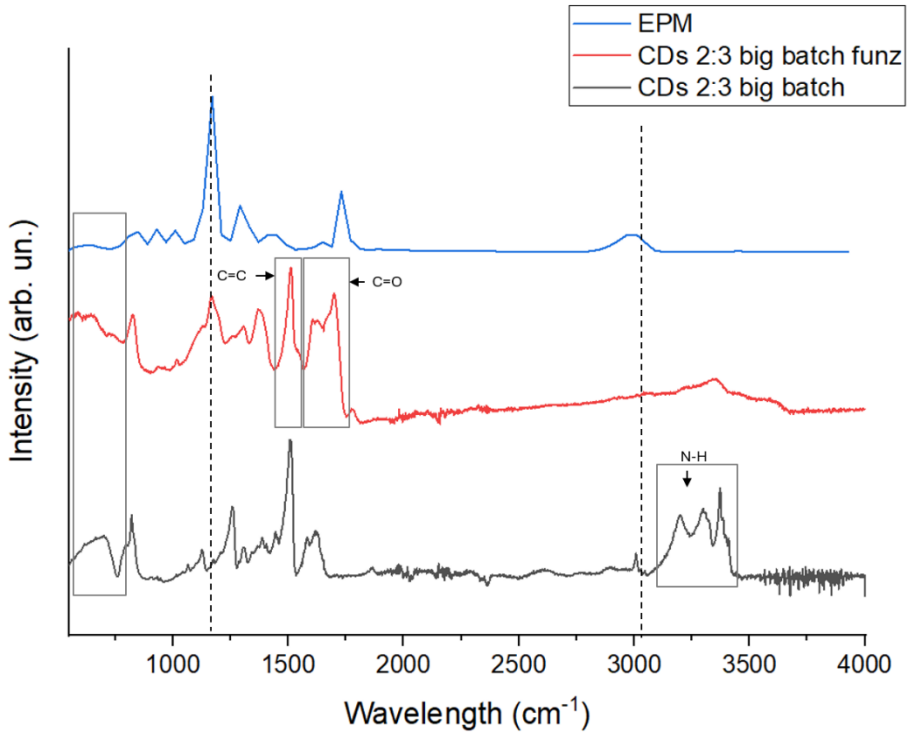

Figure 28 - Comparison of IR spectra of CDs (2:3 big batch) and F-CDs.

F-CDs spectrum (Figure 28) shows some changes caused by the functionalisation. The amine band between 3200 and 3400 cm^{-1} has completely disappeared. In the spectrum of EPM there is a peak at 1200 cm^{-1} due to the epoxide C-O bond. This peak has disappeared meaning that the NH_2 on the surface of CDs have all reacted with the epoxides of the EPM. This last reaction is very fast. The signal of the C=O groups and C=C groups that constitutes the EPM are present. At 500 and 1200 nm the signal changes due to the EPM are recognized.

All these observations suggested that the functionalisation was successful.

4.2.3 TGA

The TGA graph of **non-functionalised** CDs (Figure 31) shows four degradation phases. Between 120-340 °C there is a weight loss of 6% due to water loss. The water loss is recognisable because the weight loss is slow and continuous without significant peaks. Between 340-420 °C, there is a weight loss of 23% imputable to citric acid-like pieces (Figure 30, red fragments) and the carboxylics which degrade first because they are more fragile than the aromatic compounds. Between 420-560 °C, there is a weight loss of 21%. This degradation phase concerns the not fully aromatic parts bound by the more flexible bridges (Figure 30, violet fragments). Between 560-800 °C, there is a weight loss of 12.8%. This loss is due to the degradation of structures composed of double-bridged aromatic parts, which are stiffer than the other aromatic parts (Figure 30, blue fragments).

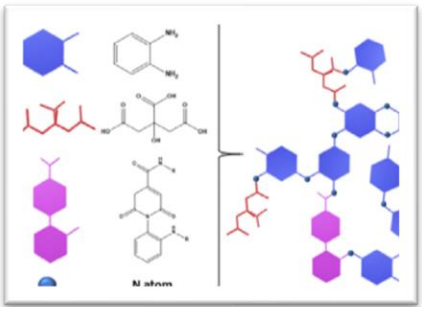

Figure 30 -Fragments of CDs. (reproduced with permission, source [101])

The TGA graph of **functionalised** CDs shows five degradation phases (Figure 32). Between 40-223 °C there is a 6% weight loss due to water loss. Between 223-280°C there is a weight loss of 12% corresponding to the loss of acrylate groups. Between 280-420°C there is a 65% weight loss related to the more brittle citric acid-like fragments. Between 420-440°C there is a 3.5% weight loss inherent to the aromatic pieces bound by flexible bridges. Between 440-800°C, there is a 5% weight loss due to the breakdown of the stronger aromatic pieces bound by double bridges.

TGA confirms that functionalisation of CDs has taken place because the same degradation steps as for the non-functionalised CDs can be recognised, plus the one between 223-280°C relating to the acrylate groups. TGA shows that the structure of CDs following functionalisation is less stable.

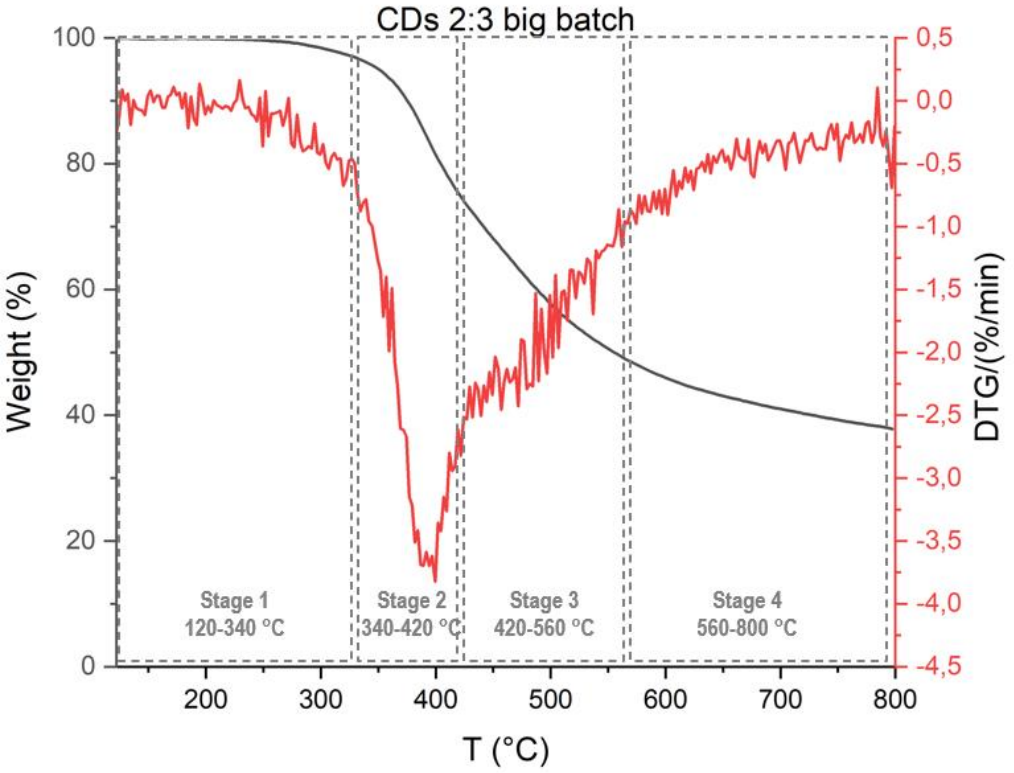

Figure 31 - TGA 2:3 CDs.

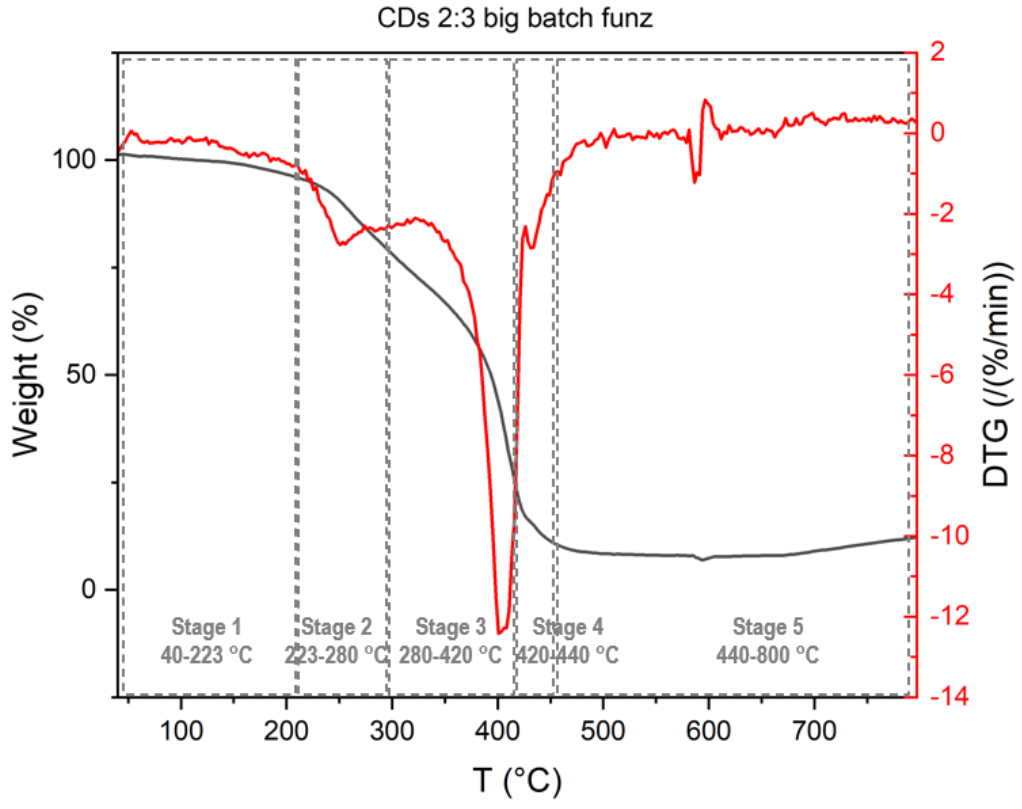

Figure 32 - TGA F-CDs.

4.2.4 AFM

CDs are the least conductive parts of the sample. In the phase-contrast images CDs are the black spots (Figure 33). Analysis of the AFM images showed that the functionalised CDs (B) have an average diameter twice as large as the non-functionalised ones (A) (Table 3).

Table 3 - Average diameter of the CDs.

	2:3 CDS	F-CDS	3:1 CDS
Average diameter (nm)	20	42	28

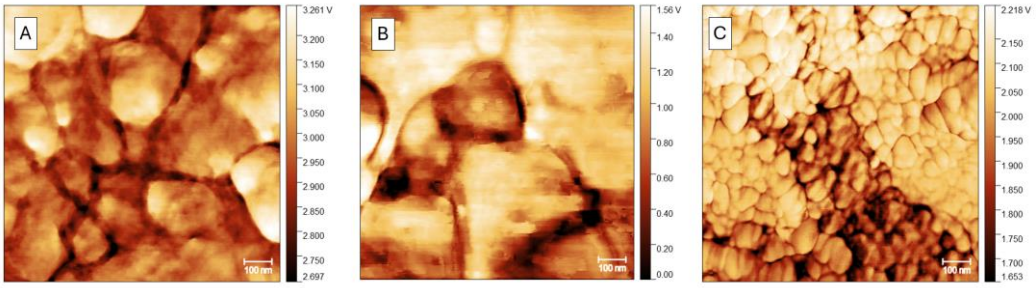

Figure 33 - AFM images of 2:3 CDs (A), F-CDs (B), 3:1 CDs (C). Scale of 100 nm.

For the sample with F-CDs, it was not possible to obtain many measurements. The stickiness of the F-CDs causes adhesion to the tip and removal from the substrate. Figure 34 shows the size distributions of the CDs. In the plots of the non-functionalised CDs (Figure 34,A,C) the distribution is unimodal, and the data are centred around the mean values given in Table 3. An increase in polydispersity due to functionalisation can be seen in Figure 34,B.

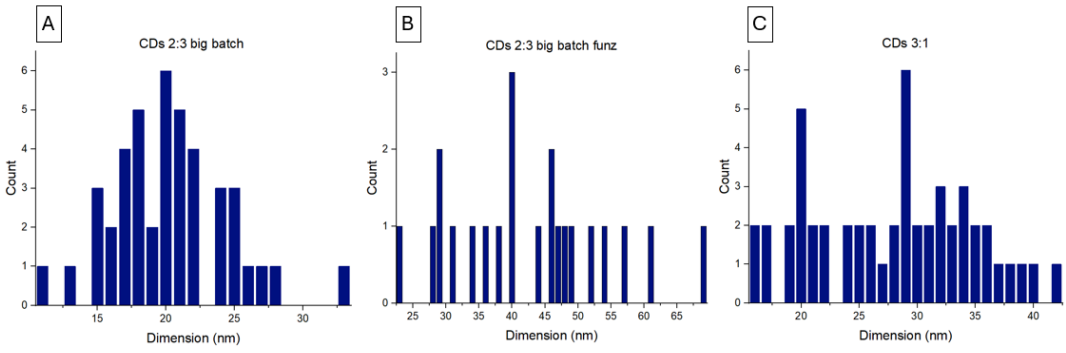

Figure 34 - Distributions of the CDs diameters.

4.2.5 UV-Vis Spectroscopy

Absorption occurs in the band between 300-380 nm. The signal at 300 nm is related to the n-π * transition of the C=O, C=N, N=N. The CDs core absorbs at about 380 nm. The absorption is mainly due to the DPA rings. By comparing the UV spectra

with the fluorescence spectra, CDs absorb and re-emit at the same wavelength. Functionalisation affects absorption, as can be seen by comparing plots A and B of Figure 35.

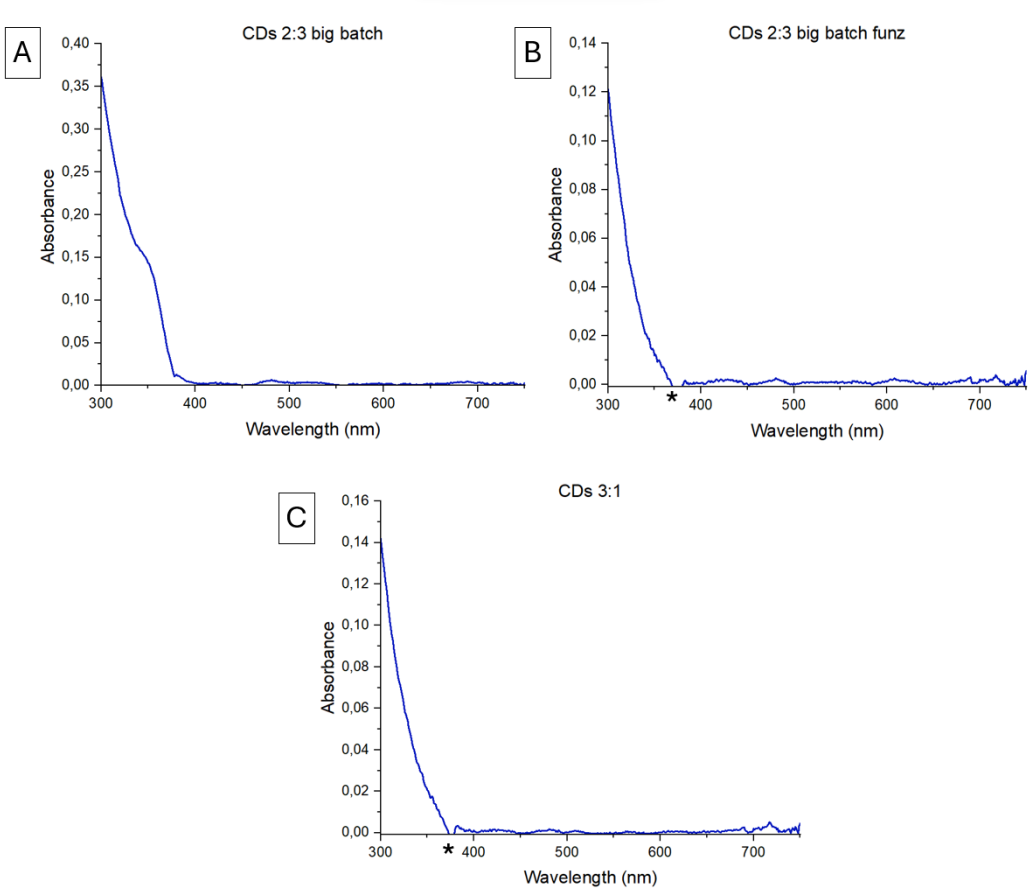

Figure 35 - UV-Vis Absorbance spectra. At the wavelength marked with an asterisk (*) the signal is interrupted because of the lamp change.

The mass extinction coefficient $\varepsilon\lambda$ was calculated using the Lambert-Beer law (Eq. 1) The absorbance A was taken as the peak value of the spectrum, the optical path l corresponded to the lateral dimension of the cuvette containing the solution (1 cm), and the concentration ρ was calculated as the mass of CDs over the solvent volume (1 mg/mL). The resulting mass extinction coefficients are given in Table 4.

Table 4 - Mass extinction coefficients.

CDs	$\varepsilon\lambda$ ($cm^{-1}mg^{-1}mL$)
(2:3) CDs	0.36
F-CDs	0.12
(3:1) CDs	0.14

4.3 Composite characterization

The acrylic groups were introduced in the CDs for chemical immobilization owing to covalent bond formation. The solutions with the F-CDs were irradiated for 15 min. The blank and the film with the non-functionalised CDs were irradiated for 30 min to achieve polymerisation. This confirms that both F-CDs and non-functionalized CDs act as chemical junctions due to the functional groups on their surface. However, the film with CDs was more fragile than the film with F-CDs. The difference in polymerization time and mechanical properties confirms that F-CDs are better candidates for film formation.

The reactive group of PEGMEMA (CH=CH2) can react by opening the double bond. PhI, when irradiated, absorbs photons that bring the molecule to an excited state. For PhI to decay from the excited state, the molecule must be broken. The rupture generates two unpaired radicals that trigger the reaction. A radical can add on the double bond of the reactive group of a monomer and generates an unpaired electron on the monomer. The generated species is a radical monomer. The unpaired electron of the radical monomer is added on the double bond of a second monomer generating the polymer. The chain reaction goes on until a termination event occurs.

Normally, photopolymerization reactions use polyfunctional monomers. When polyfunctional monomers react, they form a three-dimensional mesh in which each node is a double bond that has reacted chemically with another double bond. In this way a thermoset polymer is formed: it has chemical bonds that do not allow fusion. If **monofunctional monomers** are used, the polymerization generates a linear chain, therefore a thermoplastic polymer. In a thermoplastic polymer the chains tangle physically and not chemically.

In the case of this thesis work, the reactive groups of PEGMEMA react with each other leaving the rest of the chain as a pendant. **F-CDs are used as chemical nodes** of the polymer. The use of non-functional CDs instead of F-CDs is expected to lead to the formation of a fragile polymer.

In a photoinduced process, absorption depends on the **depth of penetration** of the radiation. For the photopolymerization to take place correctly and evenly, a thickness limit of the material is established. The limit thickness depends on how many absorbent species there are in the material. If only PhI is present as an absorbent species, the penetration of the ray is deeper. If there are CDs that can either absorb or scatter light, fewer photons pass through the material. There is a threshold depth below which there are no longer enough photons to keep the polymerization going. The 1 mm thickness chosen has resulted appropriate after experimental test.

In the radical polymerization the **oxidation** constitutes a problem. The surface layer of the material is in contact with the atmosphere oxygen, which interferes with the propagation. Therefore, a nitrogen inert atmosphere has been used and no oxidation phenomenon has been observed.

4.3.1 Fluorescence Spectroscopy

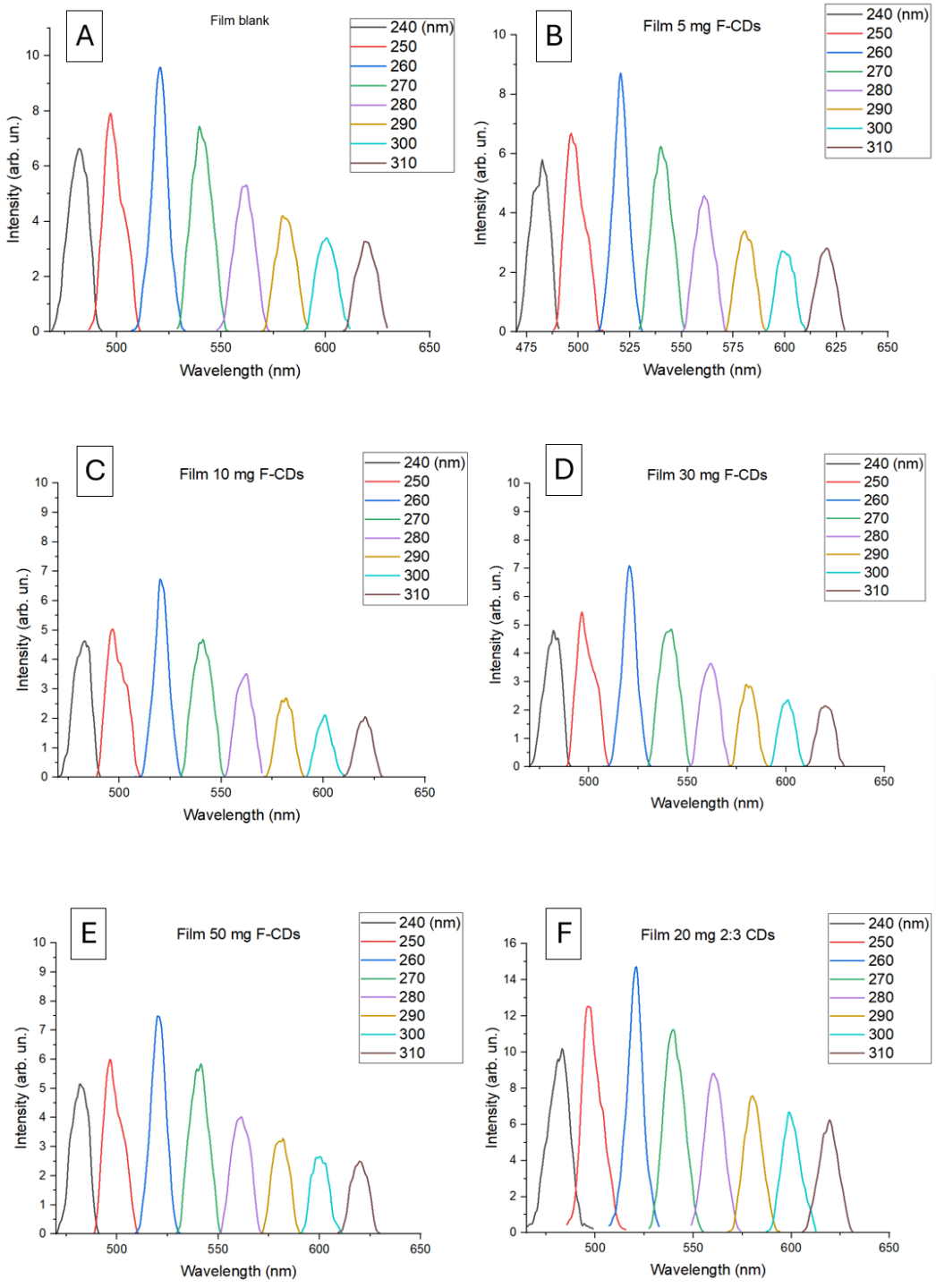

Figure 36 - Fluorescence spectra of the films.

Figure 36 shows the emissions spectra of the light-cured film. As the concentration of the F-CDs incorporated in the film increases, the fluorescence intensity decreases (B, C, D, E). The decrease in fluorescence is due to the quenching between the polymer's own fluorescence and the fluorescence centres introduced by the F-CDs

covalently bound to the polymer's chains. CDs dispersed in the unbound polymer matrix increase fluorescence emission by acting as additional fluorophores without quenching or being quenched by the polymer (F). The polymer molecules when directly bound to the CDs transfer charge to the CDs, when unbound there is no charge transfer. Several types of quenching mechanisms occur simultaneously.

4.3.2 TGA

The TGA graphs of the films were compared with those of CDs alone and the polymer alone (blank). Common peaks related to the degradation of CDs are identified. The new peaks are related to the bonds formed between CDs and the polymer. The TGA graphs of the films were also compared with the blank by which the peak of the degradation of the polymer alone is identified.

The TGA graph of **blank film** shows one degradation phase (Figure 37). Between 0-330°C there is a weight loss of 9% corresponding to the water loss. Between 0-460°C there is a weight loss of 87% corresponding to the degradation of the polymer.

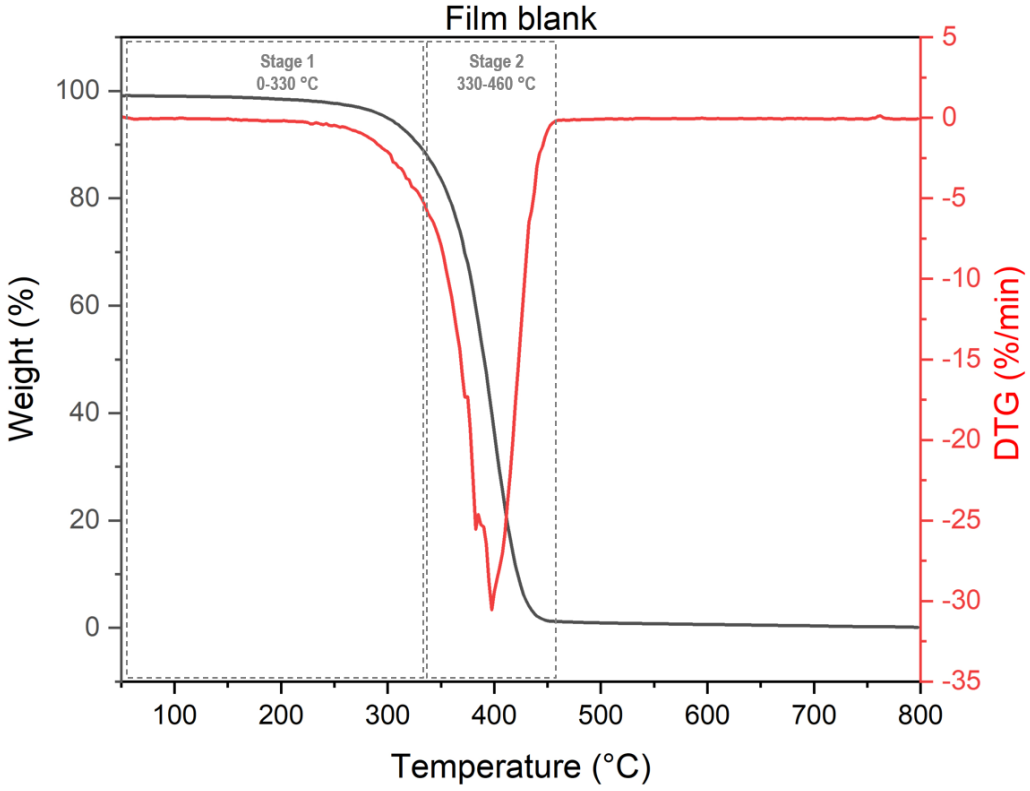

Figure 37 - Film blank.

The TGA graph of the **film with F-CDs** (4.8 wt%) shows four degradation phases (Figure 38). Between 0-320°C °C there is a weight loss of 13% due to the water loss. Between 320-360°C there is a 10% weight loss corresponding to the part of the CDs bound to the polymer. Between 360-420°C there is a 71% weight loss related to the polymer. Between 420-480°C there is a 5% weight loss related to the F-CDs. The F-CDs break down more within the film than alone (3.5%). The increment is due to the polymer rupture that creates a radical-rich environment and promotes the decomposition of the filler.

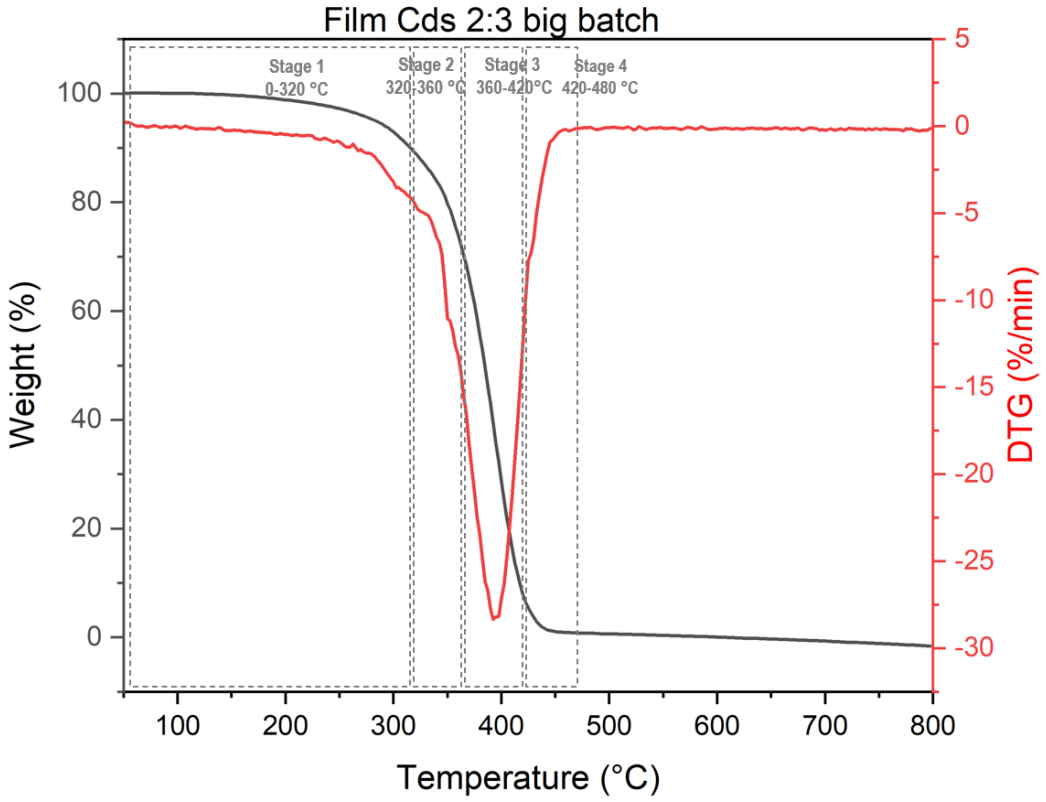

Figure 38 - Film 2:3 CDs big batch functionalised.

The TGA plot of the **film with non-functionalised CDs** shows two degradation phases (Figure 39). Between 0-390°C °C there is a weight loss of 46% related to the more brittle fragments similar to CA. CDs degradation occurs in parallel with polymer degradation. Between 390-438°C there is a 49% weight loss corresponding to the polymer. Between 438-460°C there is a weight loss of 3% corresponding to the last CDs remaining in small quantities after complete degradation of the polymer.

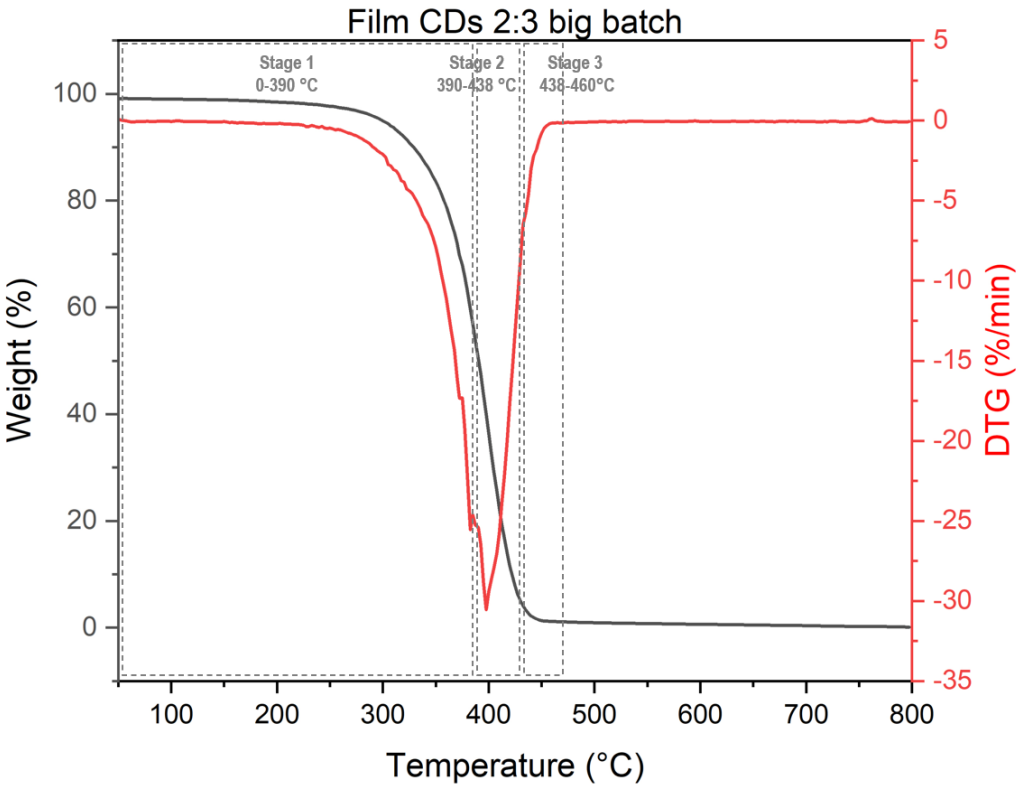

Figure 39 - Film 2:3 CDs big batch.

4.3.3 Swelling

A swelling test was used to verify the behaviour of the CDs in an aqueous environment and the possible release of CDs during the test.

The film recovered from water after 7 days lost consistency. The weight of the recovered film was not comparable with the initial weight. Hence, the variation of weight is not a significant analysis to characterize the films.

Fluorescence on the other hand, increased in every film type (Figure 40). The percentages of variation are shown in Table 5.

The increase in intensity is attributed to the interposition of water molecules between the CDs. By increasing the distance between the CDs, fluorescence quenching is reduced.

The rise in fluorescence intensity also suggests that the CDs are not easily released. This occurs not only for the F-CDs but also for the non-functionalized CDs. It follows that even the non-functionalized CDs exhibit a strong interaction with the polymer due to the functional groups on their surface.

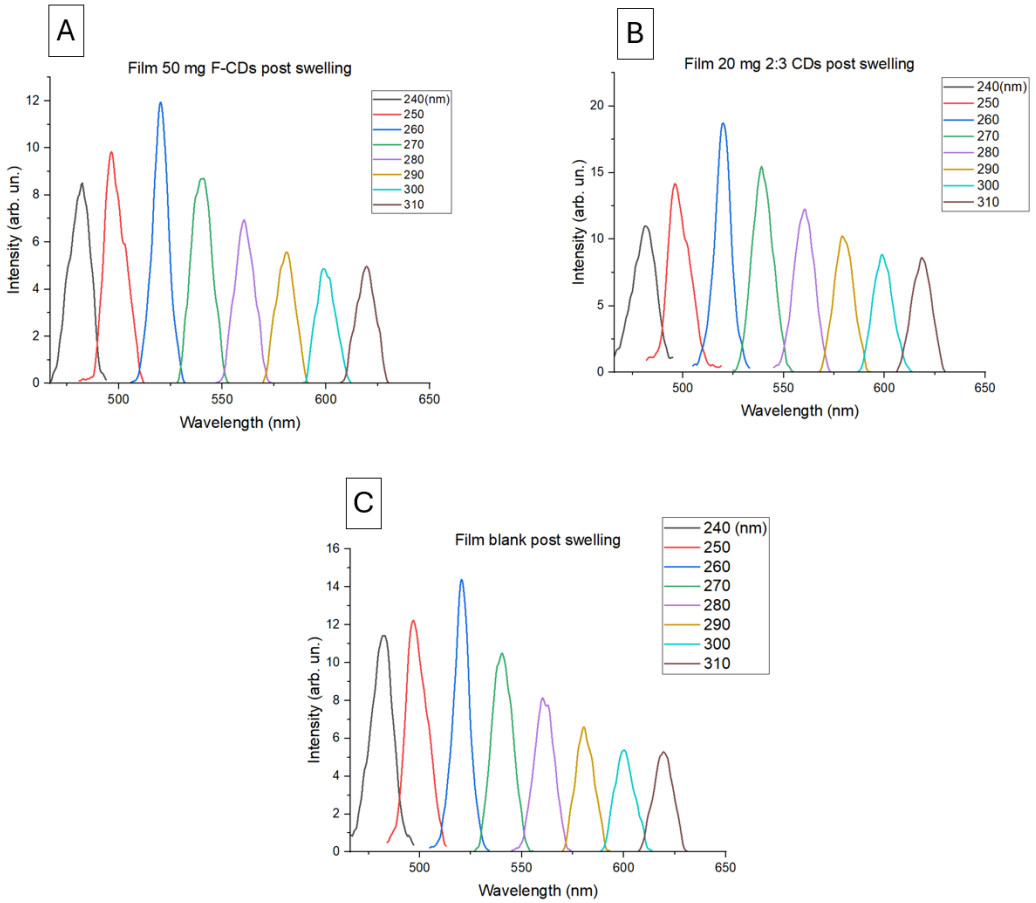

Figure 40 - Fluorescence spectra of the films post swelling.

Table 5 - Percentage variation of pre and post swelling fluorescence intensity of the maximum peak (excitation at 260 nm).

Fluorescence intensity variation due to swelling	
Film F-CDs (4.8%)	21 %
Film 2:3 CDs (1.9%)	42 %
Film blank	36 %

Conclusions

A bottom-up approach has been used for the C-Dots synthesis. The precursors in this work are DPA and CA. In the first step DPA and AC are placed in the aqueous solution and sonicated promoting in this way the aromatic heterocyclization.

The purification is performed using a dialysis membrane (1000 g/mol molecular mass cutoff). AFM analysis confirmed the nanometric size of the CDs with an average size of 20 nm for non-functionalised CDs and an average size of 40 nm after the functionalisation with EPM. It can be hypothesized that the CDs are composed by sp2 and sp3 hybridized carbon structures and present a random cross-linked polymer structures which are organized in parallel planes with external functional groups.

Fluorometer was implemented to confirm CDs photoluminescent features. CDs with a 3:1 molar ratio (CA/DPA) have the highest fluorescence intensity. However, the right compromise between fluorescence intensity and scalability of the reaction had to be found. The synthesis with a 2:3 molar ratio has emerged as the most feasible to scale up due to high fluorescence intensity and scalability of the synthesis. The resulting CDs were functionalised with EPM which enabled to expose acrylic groups on CDs surface. Comparing the normalised fluorescence maxima for non-functionalised and functionalised CDs showed a redshift of the emission peak due to the presence of the double bonds on the surface.

Comparing the FTIR spectrum of CDs with that of CA, the OH peak and the C=O peak of the free carboxyl groups have disappeared due to the reaction of CA with DPA. The peak attributed to the saturated C-H group has become less intense due to the formation of aromatic structures. Comparing the FTIR spectrum of CDs with that of DPA, the peaks related to the N-H bond has changed in intensity due to the reactions between the amine groups of DPA and the carboxyl groups of CA. FTIR analysis also showed that varying the CA-DPA molar ratio, the signals related to the aromatic part increase when there is more DPA in the CDs. The functionalisation of CDs has led to an appreciable change in the FTIR spectrum. The amine band has disappeared. The presence of the signal of C=O groups and the absence of the typical signal of free epoxides has demonstrated that the epoxides of the EPM were present and has all reacted with the NH_2 on the CDs surface.

TGA analysis has confirmed that functionalisation of CDs has taken place. The graph of non-functionalised CDs showed three main degradation phases. The first weight loss corresponds to the more fragile citric acid-like and the carboxylics bonds, the second one concerns the not fully aromatic parts bound by the more

flexible bridges and the third one is due to the degradation of stiffer structures composed of double-bridged aromatic parts. The graph of functionalised CDs showed a first degradation phase related to the acrylate groups, and the other three are the same degradation phases as for the non-functionalised CDs.

Also, absorption spectra shows that absorption occurs in the band between 300-380 nm and is mainly due to the DPA rings. By comparing the UV spectra with the fluorescence spectra, CDs absorb and re-emit at the same wavelength.

After the characterization, CDs were combined with the polymer to obtain thin films. Both films with F-CDs immobilised and films with the 2:3 CDs dispersed in the polymer were realised. Recovered films lost mechanical properties. Fluorescence increased for each type of film in varying percentages. The increase in fluorescence even for non-functional CDs indicates that they interact well with the polymer thanks to their functional groups on the surface and little is released.

The fluorometer analysis of the films with F-CDs incorporated showed that increasing the concentration of the F-CDs the fluorescence emission decreased. The decrease in fluorescence is due to the quenching between the polymer's own fluorescence and the fluorescence centres introduced by the F-CDs covalently bound to the polymer chains. 2:3 CDs dispersed in the unbound polymer matrix increased the fluorescence emission by acting as additional fluorophores without quenching or being quenched by the polymer.

TGA of the film with F-CDs confirmed the interaction between the polymer and the F-CDs. Indeed, degradation was present for both polymer-bound and individual F-CDs. An increase in degradation of the individual F-CDs was observed due to the radical-rich environment created by the rupture of the polymer.

A comparison of the films with the CDs before and after swelling shows that the fluorescence intensity increases. The intensity increase is attributed to the reduction of fluorescence quenching due to the interposition of water molecules between the CDs. Non-functionalized CDs are poorly released indicating a strong interaction with the polymer. It follows that the functionalisation may be avoided for the film preparation.

The study of thin films containing CDs could be extended by optimizing both the CDs and polymer matrix. It would be beneficial to optimize the formulation of the photopolymerized material based on its intended use, such as increasing its resistance in an aqueous environment for biological applications. This would improve control over particle release. CDs optimization can be associated with the development of a CDs library through various functionalizations and coupling strategies with different fluorophores. By modifying surface chemistry, the properties of CDs can be modulated depending on the application. With the prospect of using CDs based films *in vivo* it will be necessary to assess cytocompatibility and biocompatibility.

List of figures

Bibliography

[1] X. Xu *et al.*, “Electrophoretic analysis and purification of fluorescent single-walled carbon nanotube fragments,” *J Am Chem Soc*, vol. 126, no. 40, pp. 12736–12737, Oct. 2004, doi: 10.1021/ja040082h.

[2] Y. P. Sun *et al.*, “Quantum-sized carbon dots for bright and colorful photoluminescence,” *J Am Chem Soc*, vol. 128, no. 24, pp. 7756–7757, Jun. 2006, doi: 10.1021/ja062677d.

[3] A. B. Bourlinos, A. Stassinopoulos, D. Anglos, R. Zboril, M. Karakassides, and E. P. Giannelis, “Surface functionalized carbogenic quantum dots,” *Small*, vol. 4, no. 4, pp. 455–458, Apr. 2008, doi: 10.1002/smll.200700578.

[4] H. Li *et al.*, “Water-soluble fluorescent carbon quantum dots and photocatalyst design,” *Angewandte Chemie - International Edition*, vol. 49, no. 26, pp. 4430–4434, Jun. 2010, doi: 10.1002/anie.200906154.

[5] F. Zu *et al.*, “The quenching of the fluorescence of carbon dots: A review on mechanisms and applications,” *Microchimica Acta*, vol. 184, no. 7. Springer-Verlag Wien, pp. 1899–1914, Jul. 01, 2017. doi: 10.1007/s00604-017-2318-9.

[6] L. Cui, X. Ren, M. Sun, H. Liu, and L. Xia, “Carbon dots: Synthesis, properties and applications,” *Nanomaterials*, vol. 11, no. 12. MDPI, Dec. 01, 2021. doi: 10.3390/nano11123419.

[7] M. G. Giordano, G. Seganti, M. Bartoli, and A. Tagliaferro, “An Overview on Carbon Quantum Dots Optical and Chemical Features,” *Molecules*, vol. 28, no. 6. MDPI, Mar. 01, 2023. doi: 10.3390/molecules28062772.

[8] S. Tao, S. Zhu, T. Feng, C. Zheng, and B. Yang, “Crosslink-Enhanced Emission Effect on Luminescence in Polymers: Advances and Perspectives,” *Angewandte Chemie - International Edition*, vol. 59, no. 25. Wiley-VCH Verlag, pp. 9826–9840, Jun. 15, 2020. doi: 10.1002/anie.201916591.

[9] A. Lerf, H. He, M. Forster, and J. Klinowski, “Structure of Graphite Oxide Revisited |,” 1998. [Online]. Available: https://pubs.acs.org/sharingguidelines

[10] K. J. Mintz *et al.*, “A deep investigation into the structure of carbon dots,” *Carbon N Y*, vol. 173, pp. 433–447, Mar. 2021, doi: 10.1016/j.carbon.2020.11.017.

[11] L. Đorđević, F. Arcudi, M. Cacioppo, and M. Prato, “A multifunctional chemical toolbox to engineer carbon dots for biomedical and energy applications,” *Nature Nanotechnology*, vol. 17, no. 2. Nature Research, pp. 112–130, Feb. 01, 2022. doi: 10.1038/s41565-021-01051-7.

[12] S. Zhu, Y. Song, X. Zhao, J. Shao, J. Zhang, and B. Yang, “The photoluminescence mechanism in carbon dots (graphene quantum dots, carbon nanodots, and polymer dots): current state and future perspective,” *Nano Research*, vol. 8, no. 2. Tsinghua University, pp. 355–381, Feb. 01, 2015. doi: 10.1007/s12274-014-0644-3.

[13] J. Lu, J. X. Yang, J. Wang, A. Lim, S. Wang, and K. P. Loh, “One-pot synthesis of fluorescent carbon nanoribbons, nanoparticles, and graphene by the exfoliation of graphite in ionic liquids,” *ACS Nano*, vol. 3, no. 8, pp. 2367–2375, Aug. 2009, doi: 10.1021/nn900546b.

[14] H. Liu *et al.*, “A review of carbon dots in synthesis strategy,” *Coordination Chemistry Reviews*, vol. 498. Elsevier B.V., Jan. 01, 2024. doi: 10.1016/j.ccr.2023.215468.

[15] Y. P. Sun *et al.*, “Quantum-sized carbon dots for bright and colorful photoluminescence,” *J Am Chem Soc*, vol. 128, no. 24, pp. 7756–7757, Jun. 2006, doi: 10.1021/ja062677d.

[16] C. Kang, Y. Huang, H. Yang, X. F. Yan, and Z. P. Chen, “A review of carbon dots produced from biomass wastes,” *Nanomaterials*, vol. 10, no. 11. MDPI AG, pp. 1–24, Nov. 01, 2020. doi: 10.3390/nano10112316.

[17] M. Liu, “Optical Properties of Carbon Dots: A Review,” *Nanoarchitectonics*, vol. 1, no. 1, pp. 1–12, Jan. 2020, doi: 10.37256/nat.112020124.1-12.

[18] X. Yan, B. Li, and L. S. Li, “Colloidal graphene quantum dots with well-defined structures,” *Acc Chem Res*, vol. 46, no. 10, pp. 2254–2262, Oct. 2013, doi: 10.1021/ar300137p.

[19] B. P. Qi *et al.*, “An efficient edge-functionalization method to tune the photoluminescence of graphene quantum dots,” *Nanoscale*, vol. 7, no. 14, pp. 5969–5973, Apr. 2015, doi: 10.1039/c5nr00842e.

[20] L. Bao, C. Liu, Z. L. Zhang, and D. W. Pang, “Photoluminescence-tunable carbon nanodots: Surface-state energy-gap tuning,” *Advanced Materials*, vol. 27, no. 10, pp. 1663–1667, Mar. 2015, doi: 10.1002/adma.201405070.

[21] L. Xiao, Y. Wang, Y. Huang, T. Wong, and H. Sun, “Self-trapped exciton emission from carbon dots investigated by polarization anisotropy of photoluminescence and photoexcitation,” *Nanoscale*, vol. 9, no. 34, pp. 12637–12646, Sep. 2017, doi: 10.1039/c7nr03913a.

[22] S. R. M. Santiago, T. N. Lin, C. T. Yuan, J. L. Shen, H. Y. Huang, and C. A. J. Lin, “Origin of tunable photoluminescence from graphene quantum dots

synthesized: Via pulsed laser ablation," *Physical Chemistry Chemical Physics*, vol. 18, no. 32, pp. 22599–22605, 2016, doi: 10.1039/c6cp03159e.

[23] K. A. Ritter and J. W. Lyding, "The influence of edge structure on the electronic properties of graphene quantum dots and nanoribbons," *Nat Mater*, vol. 8, no. 3, pp. 235–242, 2009, doi: 10.1038/nmat2378.

[24] B. Ju *et al.*, "Full-colour carbon dots: Integration of multiple emission centres into single particles," *Nanoscale*, vol. 9, no. 35, pp. 13326–13333, Sep. 2017, doi: 10.1039/c7nr04576j.

[25] S. Tao, S. Zhu, T. Feng, C. Zheng, and B. Yang, "Crosslink-Enhanced Emission Effect on Luminescence in Polymers: Advances and Perspectives," *Angewandte Chemie - International Edition*, vol. 59, no. 25. Wiley-VCH Verlag, pp. 9826–9840, Jun. 15, 2020. doi: 10.1002/anie.201916591.

[26] M. J. Almendral-Parra, Á. Alonso-Mateos, S. Sánchez-Paradinas, J. F. Boyero-Benito, E. Rodríguez-Fernández, and J. J. Criado-Talavera, "Procedures for controlling the size, structure and optical properties of CdS quantum dots during synthesis in aqueous solution," *J Fluoresc*, vol. 22, no. 1, pp. 59–69, Jan. 2012, doi: 10.1007/s10895-011-0930-3.

[27] J. Xu *et al.*, "Efficient fluorescence quenching in carbon dots by surface-doped metals - Disruption of excited state redox processes and mechanistic implications," *Langmuir*, vol. 28, no. 46, pp. 16141–16147, Nov. 2012, doi: 10.1021/la302506e.

[28] P. M. Gharat, H. Pal, and S. Dutta Choudhury, "Photophysics and luminescence quenching of carbon dots derived from lemon juice and glycerol," *Spectrochim Acta A Mol Biomol Spectrosc*, vol. 209, pp. 14–21, Feb. 2019, doi: 10.1016/j.saa.2018.10.029.

[29] J. Kudr *et al.*, "Carbon dots based FRET for the detection of DNA damage," *Biosens Bioelectron*, vol. 92, pp. 133–139, Jun. 2017, doi: 10.1016/j.bios.2017.01.067.

[30] J. B. Hoffman, H. Choi, and P. V. Kamat, "Size-dependent energy transfer pathways in CdSe quantum dot-squaraine light-harvesting assemblies: Förster versus dexter," *Journal of Physical Chemistry C*, vol. 118, no. 32, pp. 18453–18461, Aug. 2014, doi: 10.1021/jp506757a.

[31] S. Liu, N. Zhao, Z. Cheng, and H. Liu, "Amino-functionalized green fluorescent carbon dots as surface energy transfer biosensors for hyaluronidase," *Nanoscale*, vol. 7, no. 15, pp. 6836–6842, Apr. 2015, doi: 10.1039/c5nr00070j.

[32] J. Huang *et al.*, "Carbon dots for all-in-one detection and degradation: The role of photoinduced electron transfer," *J Environ Chem Eng*, vol. 10, no. 6, Dec. 2022, doi: 10.1016/j.jece.2022.108951.

[33] T. Liu *et al.*, “Inner-filter Effect Induced Fluorescence Quenching of Carbon Dots for Cr(VI) Detection with High Sensitivity,” *J Fluoresc*, vol. 32, no. 6, pp. 2343–2350, Nov. 2022, doi: 10.1007/s10895-022-03028-8.

[34] Y. Zhao *et al.*, “Colloidal Chiral Carbon Dots: An Emerging System for Chiroptical Applications,” *Advanced Science*. John Wiley and Sons Inc, 2024. doi: 10.1002/advs.202305797.

[35] X. Chen *et al.*, “Recent Progress on Chiral Carbon Dots: Synthetic Strategies and Biomedical Applications,” *ACS Biomaterials Science and Engineering*, vol. 9, no. 10. American Chemical Society, pp. 5548–5566, Oct. 09, 2023. doi: 10.1021/acsbiomaterials.3c00918.

[36] N. Casado, J. Valimaña-Traverso, M. Á. García, and M. L. Marina, “Enantiomeric Determination of Drugs in Pharmaceutical Formulations and Biological Samples by Electrokinetic Chromatography,” *Critical Reviews in Analytical Chemistry*, vol. 50, no. 6. Taylor and Francis Ltd., pp. 554–584, Nov. 01, 2020. doi: 10.1080/10408347.2019.1670043.

[37] J. Geys *et al.*, “Acute toxicity and prothrombotic effects of Quantum dots: Impact of surface charge,” *Environ Health Perspect*, vol. 116, no. 12, pp. 1607–1613, 2008, doi: 10.1289/ehp.11566.

[38] S. Barman and M. Sadhukhan, “Facile bulk production of highly blue fluorescent graphitic carbon nitride quantum dots and their application as highly selective and sensitive sensors for the detection of mercuric and iodide ions in aqueous media,” *J Mater Chem*, vol. 22, no. 41, pp. 21832–21837, Nov. 2012, doi: 10.1039/c2jm35501a.

[39] H. M. R. Gonçalves, A. J. Duarte, and J. C. G. Esteves da Silva, “Optical fiber sensor for Hg(II) based on carbon dots,” *Biosens Bioelectron*, vol. 26, no. 4, pp. 1302–1306, Dec. 2010, doi: 10.1016/j.bios.2010.07.018.

[40] F. Yan, Y. Zou, M. Wang, X. Mu, N. Yang, and L. Chen, “Highly photoluminescent carbon dots-based fluorescent chemosensors for sensitive and selective detection of mercury ions and application of imaging in living cells,” *Sens Actuators B Chem*, vol. 192, pp. 488–495, Mar. 2014, doi: 10.1016/j.snb.2013.11.041.

[41] G. A. Posthuma-Trumpie, J. H. Wichers, M. Koets, L. B. J. M. Berendsen, and A. Van Amerongen, “Amorphous carbon nanoparticles: A versatile label for rapid diagnostic (immuno)assays,” *Analytical and Bioanalytical Chemistry*, vol. 402, no. 2. pp. 593–600, Jan. 2012. doi: 10.1007/s00216-011-5340-5.

[42] D. Bu, H. Zhuang, G. Yang, and X. Ping, “An immunosensor designed for polybrominated biphenyl detection based on fluorescence resonance energy transfer (FRET) between carbon dots and gold nanoparticles,” *Sens Actuators B Chem*, vol. 195, pp. 540–548, 2014, doi: 10.1016/j.snb.2014.01.079.

[43] H. Li, Y. Zhang, L. Wang, J. Tian, and X. Sun, “Nucleic acid detection using carbon nanoparticles as a fluorescent sensing platform,” *Chemical Communications*, vol. 47, no. 3, pp. 961–963, Dec. 2011, doi: 10.1039/c0cc04326e.

[44] Q. Huang *et al.*, “Carbon dots and chitosan composite film based biosensor for the sensitive and selective determination of dopamine,” *Analyst*, vol. 138, no. 18, pp. 5417–5423, Sep. 2013, doi: 10.1039/c3an00510k.

[45] Y. Zhang, X. Yang, and Z. Gao, “In situ polymerization of aniline on carbon quantum dots: A new platform for ultrasensitive detection of glucose and hydrogen peroxide,” *RSC Adv*, vol. 5, no. 28, pp. 21675–21680, 2015, doi: 10.1039/c5ra00146c.

[46] C. Yu, X. Li, F. Zeng, F. Zheng, and S. Wu, “Carbon-dot-based ratiometric fluorescent sensor for detecting hydrogen sulfide in aqueous media and inside live cells,” *Chemical Communications*, vol. 49, no. 4, pp. 403–405, 2013, doi: 10.1039/c2cc37329g.

[47] Y. Wang *et al.*, “Carbon dots of different composition and surface functionalization: Cytotoxicity issues relevant to fluorescence cell imaging,” *Exp Biol Med*, vol. 236, no. 11, pp. 1231–1238, Nov. 2011, doi: 10.1258/ebm.2011.011132.

[48] D. Bechet, P. Couleaud, C. Frochot, M. L. Viriot, F. Guillemin, and M. Barberi-Heyob, “Nanoparticles as vehicles for delivery of photodynamic therapy agents,” *Trends in Biotechnology*, vol. 26, no. 11. pp. 612–621, Nov. 2008. doi: 10.1016/j.tibtech.2008.07.007.

[49] A. Kleinauskas, S. Rocha, S. Sahu, Y. P. Sun, and P. Juzenas, “Carbon-core silver-shell nanodots as sensitizers for phototherapy and radiotherapy,” *Nanotechnology*, vol. 24, no. 32, Aug. 2013, doi: 10.1088/0957-4484/24/32/325103.

[50] C. W. Lai, Y. H. Hsiao, Y. K. Peng, and P. T. Chou, “Facile synthesis of highly emissive carbon dots from pyrolysis of glycerol; Gram scale production of carbon dots/mSiO 2 for cell imaging and drug release,” *J Mater Chem*, vol. 22, no. 29, pp. 14403–14409, Aug. 2012, doi: 10.1039/c2jm32206d.

[51] Z. Wang *et al.*, “Application of carbon dots and their composite materials for the detection and removal of radioactive ions: A review,” *Chemosphere*, vol. 287. Elsevier Ltd, Jan. 01, 2022. doi: 10.1016/j.chemosphere.2021.132313.

[52] Q. Huang, X. Lin, L. Tong, and Q. X. Tong, “Graphene Quantum Dots/Multiwalled Carbon Nanotubes Composite-Based Electrochemical Sensor for Detecting Dopamine Release from Living Cells,” *ACS Sustain Chem Eng*, vol. 8, no. 3, pp. 1644–1650, Jan. 2020, doi: 10.1021/acssuschemeng.9b06623.

[53] X. F. Wang *et al.*, “Direct white emissive Cl-doped graphene quantum dots-based flexible film as a single luminophore for remote tunable UV-WLEDs,” *Chemical Engineering Journal*, vol. 361, pp. 773–782, Apr. 2019, doi: 10.1016/j.cej.2018.12.131.

[54] J. M. Chabu, K. Zeng, G. Jin, M. Zhang, Y. Li, and Y. N. Liu, “Simple approach for the preparation of nitrogen and sulfur codoped carbon dots/reduced graphene oxide as host for high-rate lithium–]sulfur batteries,” *Mater Chem Phys*, vol. 229, pp. 226–231, May 2019, doi: 10.1016/j.matchemphys.2019.03.019.

[55] X. Zheng, G. Ding, H. Wang, G. Cui, and P. Zhang, “One-step hydrothermal synthesis of carbon dots-polymer composites with solid-state photoluminescence,” *Mater Lett*, vol. 238, pp. 22–25, Mar. 2019, doi: 10.1016/j.matlet.2018.11.147.

[56] Z. Zeng *et al.*, “Graphene Oxide Quantum Dots Covalently Functionalized PVDF Membrane with Significantly-Enhanced Bactericidal and Antibiofouling Performances,” *Sci Rep*, vol. 6, Feb. 2016, doi: 10.1038/srep20142.

[57] A. Gaikwad, M. Joshi, K. Patil, S. Sathaye, and C. Rode, “Fluorescent Carbon-Dots Thin Film for Fungal Detection and Bio-labeling Applications,” *ACS Appl Bio Mater*, vol. 2, no. 12, pp. 5829–5840, Dec. 2019, doi: 10.1021/acsabm.9b00795.

[58] M. J. Cho and S. Y. Park, “Carbon-dot-based ratiometric fluorescence glucose biosensor,” *Sens Actuators B Chem*, vol. 282, pp. 719–729, Mar. 2019, doi: 10.1016/j.snb.2018.11.055.

[59] W. H. Chen *et al.*, “Biomedical polymers: synthesis, properties, and applications,” *Science China Chemistry*, vol. 65, no. 6. Science Press (China), pp. 1010–1075, Jun. 01, 2022. doi: 10.1007/s11426-022-1243-5.

[60] D. Ozdil, I. Wimpenny, H. M. Aydin, and Y. Yang, “Biocompatibility of biodegradable medical polymers,” in *Science and Principles of Biodegradable and Bioresorbable Medical Polymers: Materials and Properties*, Elsevier Inc., 2017, pp. 379–414. doi: 10.1016/B978-0-08-100372-5.00013-1.

[61] A. Salas, M. Zanatta, V. Sans, and I. Roppolo, “Chemistry in light-induced 3D printing,” *ChemTexts*, vol. 9, no. 1, Feb. 2023, doi: 10.1007/s40828-022-00176-z.

[62] H. Samadian, H. Maleki, Z. Allahyari, and M. Jaymand, “Natural polymers-based light-induced hydrogels: Promising biomaterials for biomedical applications,” *Coordination Chemistry Reviews*, vol. 420. Elsevier B.V., Oct. 01, 2020. doi: 10.1016/j.ccr.2020.213432.

[63] H. Samadian, H. Maleki, Z. Allahyari, and M. Jaymand, “Natural polymers-based light-induced hydrogels: Promising biomaterials for biomedical applications,” *Coordination Chemistry Reviews*, vol. 420. Elsevier B.V., Oct. 01, 2020. doi: 10.1016/j.ccr.2020.213432.

[64] J. P. Fouassier, X. Allonas, and J. Lalev Ee, “0 PHOTOINITIATORS FOR FREE RADICAL POLYMERIZATION REACTIONS”, doi: 10.1.

[65] A. Albini, “Norrish’ type I and II reactions and their role in the building of photochemical science,” *Photochemical and Photobiological Sciences*, vol. 20, no. 1, pp. 161–181, Jan. 2021, doi: 10.1007/s43630-020-00003-9.

[66] M. Lee, R. Rizzo, F. Surman, and M. Zenobi-Wong, “Guiding Lights: Tissue Bioprinting Using Photoactivated Materials,” *Chemical Reviews*, vol. 120, no. 19. American Chemical Society, pp. 10950–11027, Oct. 14, 2020. doi: 10.1021/acs.chemrev.0c00077.

Acknowledgments

I would like to dedicate this space to those who, with dedication and patience, have contributed to the realisation of this thesis at the end of a long university journey.

I would like to extend a special thanks to Professor Alberto Tagliaferro, for creating a warm and welcoming working environment that inspired me to learn and grow every day and for always being available when I needed him.

I would also like to thank my supervisor, Mattia Bartoli, for the kindness and the patience with which he dealt with all the moments of crisis and his constant presence. Thank you for making me feel worthy, not only of this work, but of all the others to come.

I would like to thank my supervisor, Francesca Frascella, for her availability and advice.

I would also like to thank Ignazio Roppolo and Erik Piatti for their time and expertise, which were invaluable.

I would like to thank my colleague Miriam Ala, with whom I have shared this journey, for always being ready to lend a helping hand at every turn. I am also grateful to all the friends who have cared for and encouraged me to keep going.

Finally, I would like to thank my mother, father, and sister for being my indispensable support system to see me through to the end.